

## Evaluation of FO membranes performance using a modelling approach

Imane Chaoui<sup>a,b,\*</sup>, Issa Ndiaye<sup>a</sup>, Souad Abderafi<sup>b</sup>, Sébastien Vaudreuil<sup>a</sup>,  
Tijani Bounahmidi<sup>a</sup>

<sup>a</sup>Euro-Med Research Institute, Euro-Med University of Fes (UEMF), Rond-point Bensouda route nationale de Meknès, BP 51 Fes (Morocco), emails: i.chaoui@ueuromed.org (I. Chaoui), i.ndiaye@ueuromed.org (I. Ndiaye), s.vaudreuil@ueuromed.org (S. Vaudreuil); t.bounahmidi@ueuromed.org (T. Bounahmidi)

<sup>b</sup>Ecole Mohammadia d'Ingénieurs, Université Mohamed V de Rabat, Avenue Ibn Sina B.P 765, Rabat-Agdal (Morocco), email: abderafi@emi.ac.ma (S. Abderafi)

Received 30 November 2020; Accepted 8 February 2021

---

### ABSTRACT

Forward osmosis (FO) membranes development has made real progress over the last decade with a significant number of membranes reported in the literature. However, performances of these membranes are difficult to compare as diverse experimental conditions are used. In this study, the productivity of R&D FO membranes is predicted using a model by setting the same operating conditions, so that the water flux only depends on membranes intrinsic parameters. On this basis, a rigorous analysis of the obtained results is carried out. Membranes selectivity is discussed through the ratio of solute and water permeability coefficients. Results showed that the six best performing FO membranes in terms of water flux are thin-film composite (TFC) membranes of which four have polyvinylidene fluoride (PVDF) nanofibers support layers modified with hydrophilic materials. Advantages and limitations of different fabrication methods, membranes structures, morphologies and materials are discussed. Comparison with commercial FO membranes has also been carried out.

*Keywords:* Membranes developments; Desalination; FO membranes benchmark; Water and energy nexus; Forward osmosis.

---

### 1. Introduction

Despite the valuable efforts undertaken in terms of water management strategies and policies promoting energy efficiency, the demand for water and energy is constantly increasing. Several regions of the world suffer nowadays from water stress while a significant part of the population does not have access to safe drinking water [1]. According to the World Resources Institute (WRI), 17 countries, representing a quarter of the world's population, are currently facing extremely high water stress while 44 others are suffering from high levels of water stress [2]. The threat of water scarcity and its consequences on the economy, health and human development makes water supply issues a universal challenge. In response to this situation,

the desalination industry is expanding to more than 18,000 plants operational worldwide by 2030 to produce an estimated 54 billion m<sup>3</sup> of water per year [3]. Given that conventional desalination processes such as reverse osmosis (RO) and multistage flash distillation require an energy input representing 50% to 60% of the water production cost [4], the development of energy-efficient technologies is of great interest. Over the last decades, forward osmosis (FO) has been increasingly recognized as a promising technology, offering the possibility of using low-grade thermal energy that can be from renewable sources [5,6].

Despite the technology's potential, its development has been relatively slow since its introduction in the 1950's. This is mainly due to the limited membrane development

---

\* Corresponding author.

and the concentration polarization phenomena that have a drastic impact on the process performances [7–10]. Before commercialization of the first cellulose triacetate (CTA) FO membrane by Hydration Technology & Innovation (HTI) in 1990, osmotic processes only attracted little interest [7,8]. Prior to that dedicated membrane, RO membranes were used in the FO process, which resulted in high internal concentration polarization (ICP) and poor water fluxes [11–13]. ICP can be defined as the dilution of draw solution within the support layer of the membrane due to water diffusion, resulting in a significant decrease in osmotic gradient. Reverse solute flux (RSF) and ICP significantly reduce the osmotic pressure gradient, hence a reduction in water flux across the membrane. This represents the main FO process limitations [5,11]. With a better understanding of transport phenomena involved in osmotic processes and the development of the first thin-film composite (TFC) FO membrane by OASYS Water in 2010, performances have been greatly improved. This paved the way for a new era of membrane technologies. The last decade has seen unprecedented momentum in FO membranes R&D, with an increasing number of publications as shown in Fig. 1 [14]. The reported literature on forward osmosis membranes is mainly focused on development of new preparation methods [12,15,16], integration of nanoparticles and the use of new innovative materials [13,17–19] to improve membranes performances: productivity (water flux) and selectivity (RSF). These developments aim to improve membranes performances, namely, productivity (water flux) and selectivity (RSF). Despite the significant progress achieved in FO membrane development, its extent is hard to quantify as FO membranes performances reported are tested under diverse experimental conditions. Draw solution (DS), feed solution (FS), transmembrane pressures, temperatures and flow regimes are such parameters varying from study to study; hence making membrane performances comparison difficult.

In the present work, a benchmark of literature R&D FO membranes is carried out using productivity and selectivity as evaluation criteria. The productivity (water flux) is estimated using the study by Tiraferri et al. [20] model, while solute permeability ( $B$ ) and water permeability ( $A$ ) ratio is used as selectivity indicator. This enables the identification of the best and worst performing membranes. The various preparation methods, materials and morphologies are analyzed to identify development pathways for FO membranes with high productivity and selectivity. Finally, a comparative study of the best performing R&D FO membranes and commercial ones has been realized. Market access conditions and challenges are also discussed. This work aims to evaluate the current state of R&D FO membranes and provide guidance toward best practices.

## 2. FO process and membrane development

Forward osmosis desalination occurs as a two-steps process (Fig. 2). In the first step, water diffuses through a semi-permeable membrane from a less concentrated solution (FS) to a more concentrated solution (DS) under the effect of osmotic pressure gradient. The second stage is used to regenerate the draw solution and recover the water that has permeated. Depending on the osmotic agent, using an external energy supply is often required [5–7,21–24]. Process performances thus rely mainly on the osmotic agent and FO membrane used. Reverse solute flux (RSF) and ICP phenomena have been reported as the main technology limitations [6,23,24]. These phenomena, while linked to thermodynamic properties of the draw solute such as molecular size, solubility and diffusivity, are essentially defined by the FO membrane used [5,11,14]. A high-performance FO membrane is, therefore, essential to achieve high water flux and selectivity.

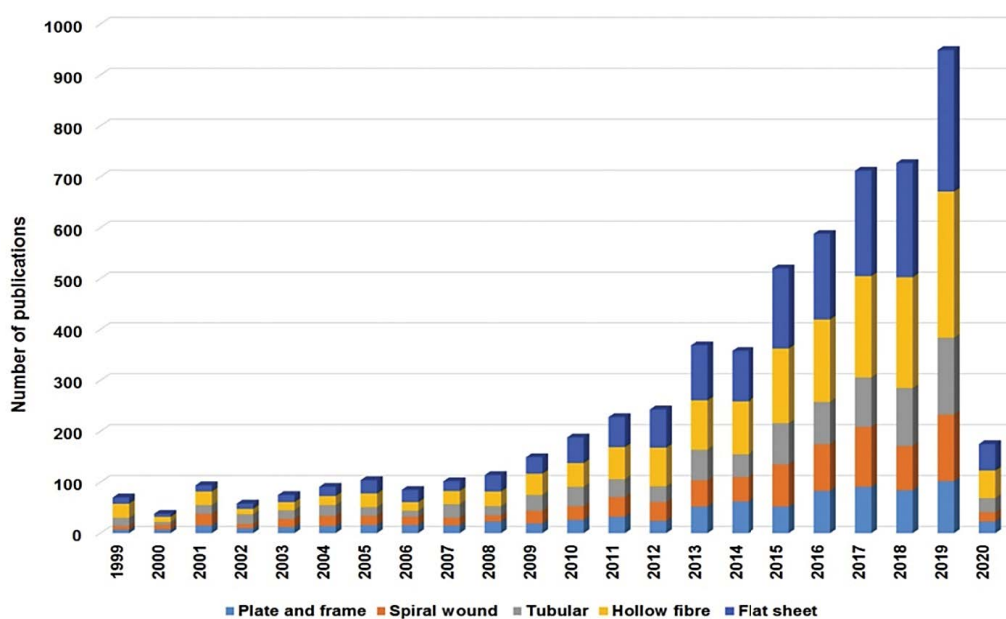


Fig. 1. Number of FO membranes publications reported in Science Direct from 1999 to 2020 [14].

### 2.1. History of membrane development

Development of osmotic processes has been relatively slow because of lack in membrane improvement since the primary membrane of the “1950s”. Membrane processes such as ultrafiltration (UF), nanofiltration (NF) and RO only established viability after production of the first asymmetric membrane in the late 1950s [25,26]. Such membrane, made by immersion precipitation (Loeb–Sourirajan Technique) [27], consists of a dense layer on top of a porous one of the same material. Asymmetric membranes have significantly improved performances of membrane processes. These membranes have shown better permeability and selectivity, resulting in low water transport resistance and operation at lower pressures [8]. Most of the asymmetric membranes are made by cellulose acetate (CA), one of the few polymers that permits the immersion precipitation technique [8,28]. CA material has, however, several limitations, including low salt retention [29], and high tendency to hydrolysis if operated outside its restricted pH range (3–7) and temperature above 35°C [11].

A breakthrough in permeability and selectivity was achieved with the first TFC membrane that outperformed asymmetric membranes [8,9,21]. As RO was the most prevalent process for desalination, TFC-RO membranes were the first membranes thus tested in FO, yielding very low water fluxes due to high ICP effects [11,29,30]. The first modelling works on transfer phenomena [7] helped researchers understand the impact of ICP on osmotic processes performances. The crucial role of the support layer, previously considered to have only a mechanical function, on ICP phenomena has also been highlighted [5,8]. In the “90s”, the introduction by HTI of the first CTA membrane made specifically for FO processes helped research gain traction, especially the optimization of support layer properties. The first TFC-FO membrane with significant increase of performances was commercialized in 2010 by OASYS Water [31]. This paved the way for a new era in FO membrane development, resulting in the emergence of several companies manufacturing and commercializing membranes for FO applications. Today’s main suppliers of FO membranes are Porifera, Toyobo, Aquaporin, Trevi Systems, Fluid Technology Solutions (FTSH2O) (2482 SW Ferry St., Albany, OR97322, USA), Oasys Water and Modern Water, mainly manufactures TFC and CTA membranes [32].

### 2.2. FO membranes

FO membranes are typically asymmetric, we can distinguish asymmetric phase inversion membranes

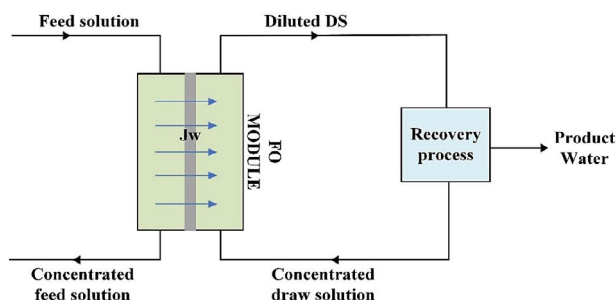


Fig. 2. FO process schematic description.

and composite membranes [5]. While fully asymmetric membranes are prepared by immersion precipitation (e.g., phase separation induced by a non-solvent) and consist of a single material, composite membranes consist of different materials structured as a selective layer over a support layer. The membrane support layer is generally prepared by immersion precipitation [33–35], temperature-induced phase separation [36,37] or electrospinning [19,38–40] while the active layer is made by interfacial polymerization (IP) [29,41,42] or through layer-by-layer (LBL) deposition [43,44]. Various materials can be used to prepare FO membranes. For asymmetric membranes, most used materials are cellulose (CA, CTA) and polybenzimidazole (PBI).

Because of its hydrophilic properties and good chemical and mechanical stabilities, PBI was one of the first materials used in fully asymmetric FO membranes; the first PBI-FO membrane has been developed by Wang et al. [45]. Other PBI-FO membranes have been synthesized, including some chemically treated with p-xylylene dichloride [46] or PBI/polyethersulfone (PES) membranes obtained by co-extrusion [47]. Cellulose, also used for FO membranes, is an inexpensive hydrophilic material with good mechanical properties [28]. Several works on the development of cellulosic membranes for FO applications have been reported in the literature [28,48–52]. Wang et al. [48] have prepared and tested membranes made from CA while cellulose ester (CE) membranes have been synthesized by Ong et al. [52]. The main limitations of cellulosic and PBI membranes remain the relatively low water flux. PBI membranes also demonstrate low retention of monovalent salts.

TFC membranes are the most commonly used membranes in FO due to their higher performances. Several materials such as polysulfone (PSf), PES, PVDF, polyacrylonitrile (PAN) [29,39,42,53] have already been used for the support layer of TFC membranes. The selective layer consists on the other hand of a PA layer prepared by IP generally from 1,3-phenylenediamine (MPD) and trimethylene carbonate (TMC) monomers [41]. The first TFC-FO membrane marketed by Oasys Water was inspired by the work of Phillip et al. [29], who synthesized for the first time an optimized TFC membrane to achieve better FO performances. To improve FO performances, the support layer of the membrane was made of PSf on which a layer of PA was deposited by IP. A number of studies [54–59] later focused on physical or chemical modifications to the different layers to improve performances. Obaid et al. [59] incorporated SiO<sub>2</sub> nanoparticles into PVDF substrates. Ghanbari et al. [60] modified the active layer of the membrane by adding nanoparticles of HNTs during the preparation of the aqueous solution for IP. Liang et al. [56] integrated aquaporin proteins into the selective layer of a TFC membrane made from PSf substrate to improve its permeability. The concept of chemically modifying the surface of the support layer or active layer was also investigated by researchers [54,55,61]. These are electrically charged membranes, which their selection mechanism is dominated by the Donnan effect [62], making them a poor candidate for FO desalination.

Recently, Li et al. [63] have prepared by evaporation-induced phase separation an integrally symmetrical membrane for the FO process. With a zero structural parameter (*S*), identical performances were obtained for

both orientation modes meaning no ICP. Smart FO membranes with pH-responsive properties were also recently investigated. Salehi et al. [64] synthesized a polysulfone-graft-poly(2-dimethylaminoethyl methacrylate) (PSf-g-PDMA), where the pH-responsive co-polymer was blended with PSf during the phase inversion process of the support layer preparation, followed by IP to form the active layer. Authors reported pH-reversibility as higher water fluxes were achieved in acidic pH (3) than in basic pH (10). This was explained by protonation of the -N(Me)<sub>2</sub> groups covering the supports layer pore surfaces, leading to an increase in the osmotic pressure gradient in FO mode. Ceramic-based FO membranes have also been explored for improved mechanical, chemical and thermal stability. Zhang et al. [16] have prepared a mullite ceramic substrate coated by a TiO<sub>2</sub>/CNT interlayer to overcome the low porosity and coarse surface of the ceramic substrate to allow the PA layer formation. Authors reported good membrane selectivity and water flux (<5 g/m<sup>2</sup>h, ~19 LMH).

Table 1 gives materials, preparation methods, intrinsic parameters, experimental water flux and RSF corresponding to each FO membrane.

### 3. Benchmark of FO membranes performances methodology

#### 3.1. FO model description

An FO membrane is considered to be high-performance depending on its ability to achieve a high water flux while restricting the passage of solutes. These performance indicators depend both on the membrane and the draw and feed solution properties. FO literature membranes being tested under various DSs, FSs and operating conditions, it is difficult to make a comparison based on the reported experimental data. The same testing conditions should, therefore, be used in order to compare membranes' performances. To do so, a modelling approach has been adopted to compare FO membranes performance.

Several models for water flux prediction in FO are proposed in the literature [8,25,65–68], but most do not account for all phenomena taking place in a FO process such as the concentration polarization (CP) and reverse solute flux (RSF). Tiraferri et al. [20] proposed a model to predict water flux in FO mode that accounted for the various phenomena involved in the FO process. The resulting water flux equation,  $J_w$  is expressed as follows:

$$J_w = A \left\{ \frac{\pi_D \exp\left(-\frac{J_w S}{D}\right) - \pi_F \exp\left(\frac{J_w}{k}\right)}{1 + \left(\frac{B}{J_w}\right) \left[ \exp\left(\frac{J_w}{k}\right) - \exp\left(-\frac{J_w S}{D}\right) \right]} \right\} \quad (1)$$

where  $\pi_F$  and  $\pi_D$  are the osmotic pressures of the feed and draw solutions, respectively;  $k$  is the mass transfer coefficient and  $D$  is the solute diffusivity and  $A$ ,  $B$  and  $S$  are the membranes intrinsic parameters.

In this model, the terms  $\exp(J_w/k)$  and  $\exp(J_w S/D)$  take into account the ECP and ICP respectively, while the term  $1/[1+(B/J_w)[\exp(J_w/k)-\exp(-J_w S/D)]]$  takes into

account the back diffusion of solutes across the membrane. The parameters  $A$  and  $B$  measure the capacity of the membrane to allow water molecules and solutes passage, respectively. The structural parameter,  $S$ , is given by the following expression:

$$S = \frac{\tau \times \delta}{\epsilon} \quad (2)$$

Eq. (2) shows that the  $S$  parameter is a function of tortuosity ( $\tau$ ), thickness ( $\delta$ ) and porosity ( $\epsilon$ ) of the support layer, which can also be considered as a measure of ICP [69]. ICP is known to be the main cause of reduced osmotic water flux, especially when the membrane is oriented in FO mode [5,66].

Many research groups [20,70–72] have already used this model in their work and shown its reliability. First, by testing different membranes, Tiraferri et al. [20] showed that the model predicted water flux with good accuracy. Later, Xiao et al. [70] prepared two different TFC membranes using PSf as substrate and PA as active layer. The membranes were tested at various DS concentrations (0.5 – 4 M NaCl) with DI water as FS. Authors found a good agreement between the water flux calculated using the model and experimental measures over the entire concentration range of DS. Boo et al. [71] tested two commercial HTI membranes using different DSs (trimethylamine-carbon dioxide (TMA-CO<sub>2</sub>), ammonia-carbon dioxide (NH<sub>3</sub>-CO<sub>2</sub>) and NaCl) against DI water as FS. Experimental results were successfully compared with those calculated using the model. Pan et al. [72] developed a self-sustained TFC membrane using PAN nanofiber as substrate and PA active layer (PA/PAN-eTFC). Authors also obtained good agreement between model predictions and experimental data. Comparison between experimental and calculated data (Fig. 3) shows a high correlation coefficient of 99.8%. The model predicts water flux with good accuracy; the average absolute error is equal to 2.6% and does not exceed 4.4% as shown in Table 2.

#### 3.2. Calculation procedure

The model given in Eq. (1) is used to predict membranes water flux. It was solved numerically, using Levenberg–Marquardt iterative algorithm [75], using Python software, following procedure presented in Fig. 4. NaCl being the reference DS in all FO experiments due to its numerous advantages, namely, high osmotic properties, high water solubility, abundance, low cost and non-toxic, it has been selected as DS [11,76]. In addition to that, most FO membranes intrinsic parameters have been defined for NaCl [11]. The osmotic pressure and diffusivity of the DS (1 M NaCl) were taken from the literature and are equal to 48 atm and  $1.41 \times 10^{-9}$  m/s, respectively [71]. Thermodynamic properties of DI water as FS and 1 M NaCl as DS were used for a temperature of 25°C. Under these conditions, the water flux equation only depends on the intrinsic parameters characterizing each membrane. The mass transfer coefficient was assumed infinite, thereby neglecting any ECP effects. This assumption implies that negligible FS concentrations are implemented in the FO

Table 1  
Summary of literature FO membranes

Year	Designation	Membranes	Materials	Preparation	Draw solution (DS)	Water flux in FO mode (LMH)	RSF (gMH)	Intrinsic parameters			Ref.
								A (LMH/bar)	B (LMH)	S (µm)	
2007	M1	NF hollow fiber membrane	PBI	Dry-jet wet phase inversion	DI water (2.0 M MgSO <sub>4</sub> )	5.65	–	0.5	–	–	[45]
2009	M2	Dual-layer NF hollow fiber membrane	PBI-PES	Co-extrusion	ED (5 M MgCl <sub>2</sub> )	24.2	0.45	1.74	–	–	[47]
2009	M3	NF hollow fiber membrane with thin wall	PBI	Phase inversion, chemical cross-linking by p-xylylene	DI water (5 M MgCl <sub>2</sub> )	20	–	1.53	–	–	[46]
2010	M4	Double skinned flat sheet	CA	Phase inversion, thermal annealing at 85°C for 15 min	DI water (5 M MgCl <sub>2</sub> )	48.2	6.5	0.78	0.46	–	[48]
2010	M5	Double dense-layer	CA	Phase inversion	DI water (2 M NaCl)	~7.5	~3.75	0.17	0.07	–	[28]
2010	M6	Hollow fiber NF	CA	Dry-jet wet spinning process	DI water (2 M MgCl <sub>2</sub> )	5	–	0.47	–	–	[50]
2011	M7	Flat sheet	CE	Phase inversion	Seawater (1.5 M NaCl)	5	–	1.3	–	–	[49]
2011	M8	Flat-sheet composite	CA on nylon fabric support	Phase inversion in water	35 g/L NaCl (150 g/L MgSO <sub>4</sub> )	1.3	–	0.13	–	–	[51]
2012	M9	Molecularly designed cellulose ester	CE	Phase inversion	DI water (2 M NaCl)	~12.3 (CAP-L)	~6.8	0.43	0.44	–	[52]
2010	M10	Flat-sheet TFC	PSf-support, PA active layer	Phase inversion, interfacial polymerization	DI water (1.5 M NaCl)	~18.1	–	1,146	–	492	[29]
2010	M11	Hollow fiber	PES hollow fiber, PA active layer	Dry-jet wet spinning method, interfacial polymerization	DI water (0.5 M NaCl)	5 (#A-FO) 14 (#B-FO)	2.12 1.75	0.95 2.193	0.29 0.2	1,370 595	[42]

(continued)

Table 1 Continued

Year	Designation	Membranes	Materials	Preparation	Draw solution (DS)	Water flux in FO mode (LMFH)	RSF (gMH)	Intrinsic parameters			Ref.
								A (LMH/bar)	B (LMH)	S ( $\mu\text{m}$ )	
2010	M12	Hollow fiber	PES hollow fiber, PA active layer	Dry-jet wet spinning method, interfacial polymerization	0.59 M NaCl (2 M NaCl) DI water (0.5 M NaCl)	12.4 42.6	0.967 4	3.46	0.22	550	[117]
2011	M13	Flat-sheet TFC	PES nano-fiber support, PA active layer	Electrospinning, interfacial polymerization	–	–	–	–	–	–	[107]
2011	M14	Flat-sheet TFC	PSf porous substrates, PA active layer	Phase inversion, interfacial polymerization	10 mM NaCl (0.5 M NaCl)	12 (TFC-2)	~5	1.78	0.356	670	[118]
2011	M15	Flat-sheet TFC	PES-sulfonated polymer substrate, PA active layer	Phase inversion, interfacial polymerization	DI water (2 M NaCl)	21 (50 wt.% sulfonated polymers)	2.2 (50 wt.% sulfonated polymers)	0.73	0.25	324	[119]
2011	M16	Flat-sheet TFC	PES nano-fiber support, PA active layer	Electrospinning, interfacial polymerization	–	–	–	–	–	–	[38]
2011	M17	Nanoporous flat sheet	PES cast on PET fabric	Phase inversion	DI water (3 M NaCl)	30	~7 mol/m <sup>2</sup> h	–	–	–	[120]
2012	M18	Macrovoid-free TFC hollow fiber	PES hollow fiber support, PA active layer	Phase inversion, interfacial polymerization	DI water (2 M NaCl)	34.5	–	1.83	0.348	261	[121]
2012	M19	Flat-sheet TFC	SPEK substrate, PA active layer	Wet phase inversion, interfacial polymerization	Model seawater (2 M NaCl) DI water (2 M NaCl)	17 35 (50 wt.% SPEK with DEG)	– 7 (50 wt.% SPEK with DEG)	0.75	0.068	107	[97]
2012	M20	Zeolite-polyamide thin film nanocomposite	PSf support, PA active layer incorporated with NaY zeolite nanoparticles	Phase inversion, interfacial polymerization	10 Mm NaCl (1 M NaCl)	15 (TFN0.1 wt/v% zeolite loading)	~3	2.58	1.58	–	[122]

2012	M21	Flat-sheet TFC	PSf-support, PA active layer with fine-tuned nanoparticles	Non-solvent (water)-induced phase separation, interfacial polymerization	-	-	-	-	-	[33]
2013	M22	Flat sheet TFC	Carboxylated Polysulfone (CPSf) substrate, PA active layer	Phase inversion, lithiation procedure, interfacial polymerization	DI water (1 M MgCl <sub>2</sub> )	18	2.2	-	-	[123]
2013	M23	Flat sheet TFC	Sulfonated polyphenylene sulfone (sPPSU) substrate, PA active layer	Direct synthesis route with various content of sulfonated units, interfacial polymerization	DI water (2 M NaCl)	48 (2.5 mol% sDCDPS)	7.6 (2.5 mol% sDCDPS)	3.23	1.05	652
2013	M24	Thin-film nano-composite	PSf support, PA active layer, amine F-MWCNTs as additives in MPD solution	Phase inversion, interfacial polymerization	10 mM NaCl (2 M NaCl)	40 (0.1 F-MWCNT wt/MPD vol.%) 30 (0.5 0.1 F-MWCNT wt/MPD vol.%)	~3 2.5	4.47 3.6	0.17 0.103	410 380
2013	M25	TFC membrane	Polyvinylidene fluoride (PVDF) nanofiber substrate, PA active layer	Electrospinning, interfacial polymerization	DI water (1 M NaCl)	28	12.9	3.15	2.33	325
2014	M26	Thin-film nano-composite flat sheet	PSf-TiO <sub>2</sub> nano-composite substrate, PA active layer	Phase inversion, interfacial polymerization	DI water (2 M NaCl) DI water (0.5 M NaCl)	33 (0.6 wt.% TiO <sub>2</sub> loading) 18.8 (0.6 wt.% TiO <sub>2</sub> loading)	15.7 (0.6 wt.% TiO <sub>2</sub> loading) 7.35 (0.6 wt.% TiO <sub>2</sub> loading)	2.63	2.19	390
2014	M27	Thin-film nano-composite flat sheet	PSf-TiO <sub>2</sub> nano-composite substrate, PA active layer	Phase inversion, interfacial polymerization	10 mM NaCl (2 M NaCl)	30 (0.5 wt.% TiO <sub>2</sub> loading)	7.5 (0.5 wt.% TiO <sub>2</sub> loading)	1.96	0.38	420

(continued)

Table 1 Continued

Year	Designation	Membranes	Materials	Preparation	Draw solution (DS)	Water flux in FO mode (LMH)	RSF (gMH)	Intrinsic parameters			Ref.
								A (LMH/bar)	B (LMH)	S ( $\mu\text{m}$ )	
2014	M28	Thin-film nanocomposite	PSf support, PA active layer containing silica nanoparticles	Phase inversion, interfacial polymerization	10 mM NaCl (2 M NaCl)	~15 (0.05 wt/vol.% silica loading)	1.5	3.436	1.025	368	[58]
2014	M29	Flat sheet TFC	PSf-SPPO substrate, PA active layer	Phase inversion, interfacial polymerization	DI water (2 M NaCl)	39	6.1	3.55	0.74	293 $\pm$ 22	[80]
2015	M30	GO/Ag nano-composite functionalized membrane	Go/Ag bonded on PA HTI TFC	Hummers' method, chemical reduction, chemical crosslinking	DI water (1 M NaCl)	~5	-	1.4	0.4	-	[125]
2015	M31	Flat-sheet TFC	Layered silica-PSf mixed matrix substrate, PA active layer	Phase inversion, interfacial polymerization	DI water (1 M NaCl)	27.4 (TFC-S2)	11.6 (TFC-S2)	1.99 $\pm$ 0.07	1.35 $\pm$ 0.4	218 $\pm$ 17	[34]
2015	M32	Thin-film nanocomposite flat sheet	PSf support layer, PA active layer containing NH <sub>2</sub> -TNTs	Phase inversion, interfacial polymerization	10 mM NaCl (0.5 M NaCl)	17.82 (0.05 wt.% NH <sub>2</sub> -TNT)	2.17 (0.05 wt.% NH <sub>2</sub> -TNT)	2.39	0.37	-	[85]
2015	M33	Molecular layer-by-layer assembly membrane	HPAN support layer, PEI/PAA interlayer, PA active layer	Layer-by-layer deposition	DI water (0.5 M NaCl)	24.6 $\pm$ 0.8	2.36 $\pm$ 0.7	2.72 $\pm$ 0.06	1.07 $\pm$ 0.10	350 $\pm$ 30	[126]
2015	M34	Zn <sub>2</sub> Ge nanowire-modified membrane	Zn <sub>2</sub> Ge nanowire modified PES substrate, PA active layer	Phase inversion, interfacial polymerization	DI water (2 M NaCl)	~21	~4	2.47 $\pm$ 0.77	8.4	540	[35]
2015	M35	Flat-sheet TFC	PSf/GO substrate, PA active layer	Phase inversion, interfacial polymerization	DI water (0.5 M NaCl)	19.77 (0.25 wt.% loading)	~3.3	1.76	0.19	191	[127]

2015	M36	Flat-sheet TFC	PES-CN/rGO nanocomposite substrate, PA active layer	Phase inversion, interfacial polymerization	DI water (1 M NaCl)	~35 (0.5 wt.% CN/rGO)	~125 mmol/m <sup>2</sup> h	1.59	0.329	163	[128]
2015	M37	Dual selective TFC membrane	PA bottom layer, CE porous support, PA top layer	Phase inversion, interfacial polymerization	DI water (1 M NaCl)	34.5 ± 1.7	3.5 ± 0.6	0.98 ± 0.01	0.09 ± 0.01	52 ± 8	[101]
2015	M38	TFC membrane	PSf support layer, PA active layer	Co-casting phase inversion process, interfacial polymerization	DI water (0.5 M NaCl)	20.1	~2.12	1.65 ± 0.06	0.12 ± 0.05	167 ± 16	[70]
2015	M39	CTA membrane	Cellulose triacetate, carboxylated carbon nanofiber	Phase inversion process	10 mM NaCl (1 M NaCl)	15.6 ± 0.5	0.9 ± 0.2	2.1 ± 0.15	0.94 ± 0.054	600 ± 50	[129]
2015	M40	Double-skinned hollow fiber membrane	PES support, PA RO-like skin-layer, PSS/PAH NF-like outer skin layer	Phase inversion, interfacial polymerization, layer-by-layer	DI water (0.5 M NaCl)	32.7	3.6	2.01	0.16	–	[130]
2015	M41	Thin-film nanocomposite membrane	PSf support layer, PA active layer containing HNTs	Phase inversion, interfacial polymerization	10 mM NaCl (2 M NaCl)	20.1	~6	1.86	0.63	–	[60]
2015	M42	Flat-sheet TFC-FO membranes	CAP support layer, PA active layer	Phase inversion, interfacial polymerization, Post-treatment	DI water (1 M NaCl)	56.9 ± 1.8	7.8 ± 0.6	2.85	0.345	31.9	[131]
2015	M43	PAN supported TFC hollow fiber membrane	PAN support layer, PA active layer	Dry-jet-wet spinning, interfacial polymerization	DI water (1 M NaCl)	17.01	6	1.96	0.7	499	[132]
2015	M44	Nanofiber TFN membrane	CNTs-incorporated PEI support layer, PA layer	Electrospinning, interfacial polymerization	DI water (1 M NaCl)	32.8	3.94	2.6	0.7	210	[19]

(continued)

Table 1 Continued

Year	Designation	Membranes	Materials	Preparation	Draw solution (DS)	Water flux in FO mode (LMH)	RSF (gMH)	Intrinsic parameters			Ref.
								A (LMH/bar)	B (LMH)	S ( $\mu\text{m}$ )	
2015	M45	TFC membrane	Polyketone-substrate, PA layer	Phase inversion, interfacial polymerization	DI water (0.6 M NaCl)	24.4	0.057 mol/ $\text{m}^2\text{h}$	2.5	0.18	280	[133]
2015	M46	CTA/CA-based membrane containing boehmite hydrophilic nanoparticles	CTA/CA	Phase inversion	DI water (1 M NaCl)	15 $\pm$ 0.5	2.5	1.43 $\pm$ 0.05	0.18	530 $\pm$ 50	[134]
2016	M47	TFC surface modified PVDF nanofiber	Surface modified PVDF nanofiber support-PA active layer	Electrospinning, interfacial polymerization	ED (1 M NaCl)	22	3.74	1.28	0.25	193	[54]
2016	M48	Thin-film nanocomposite	Silica nanoparticles embedded in polyetherimide (PEI) nanofibrous support, PA active layer	Electrospinning, interfacial polymerization	DI water (1 M NaCl)	42 (1.6 wt.% silica)	~5.04 (1.6 wt.% silica)	2.99 $\pm$ 0.11	0.44 $\pm$ 0.12	174 $\pm$ 36	[86]
2016	M49	Thin-film nanocomposite	LDH-blended PSf substrate, PA active layer	Phase inversion, interfacial polymerization	DI water (1 M NaCl)	18.1 (2 wt.% LDH-NPs)	8.1 (2wt.% LDH-NPs)	0.61	0.27	148	[84]
2016	M50	Thin film composite (TFC)	PES substrate, PA active layer crosslinking with EDA or SEA	Phase inversion, interfacial polymerization, Chemical crosslinking	DI water (2 M NaCl) DI water (1 M NaCl)	~ 17 (SEA) ~13.75 (SEA)	– –	0.559 $\pm$ 0.205	0.416 $\pm$ 0.344	301 $\pm$ 11	[113]
2016	M51	Thin-film nanocomposite flat sheet	Polysulfone/halloysite nanotubes (PSf-HINTs) nanocomposite substrate, PA active layer	Phase inversion, interfacial polymerization	10 mM NaCl (2 M NaCl)	27.7 (0.5 wt.% HINTs)	14.62 (0.5 wt.% HINTs)	2	0.337	370	[135]

2016	M52	Flat-sheet double skinned TFC	PSf mesh incorporated double skinned substrate with bottom surface hydrophilized with polydopamine(PDA), PA active layer	Phase inversion, hydrophilization deposited PDA into the bottom surface of the double skinned substrate, interfacial polymerization	-	-	-	-	-	[136]
2016	M53	Amorphous SiO <sub>2</sub> Nps-incorporated PVDF nanofiber membrane	PVDF/SiO <sub>2</sub> composite nanofiber substrate, PA active layer	Electrospinning, interfacial polymerization	Fresh water (2 M NaCl)	83 (0.5 wt.% SiO <sub>2</sub> )	1.36	0.884	29.7 ± 0.6	[59]
2017	M54	TFC membrane	PI nanofiber support layer, PA active layer	Electrospinning, first IP procedure, secondary IP procedure	DI water (1 M NaCl)	12 ± 0.9 (PIN-2-2) 12.3 ± 0.9 (PIN-2-1) 13.6 (PIN-2-0)	1.9 ± 0.6 4.1 ± 1.5 4.7 ± 0.8	11.6 ± 1.2 18.8 ± 2 28 ± 4.1	434 378 350	[137]
2017	M55	Thin-film nanocomposite membrane	PES-ZnO-SiO <sub>2</sub> core shell nanoparticles (ZSCSNPs) substrate, PA active layer	Phase inversion, interfacial polymerization	DI water (1 M NaCl)	33.5 (1 wt.% ZSCSNPs)	~12 (1 wt.% ZSCSNPs)	4.01	297	[13]
2017	M56	Hollow fiber TFC membrane	Poly ketone support layer, PA active layer	Non-solvent induced phase inversion, interfacial polymerization	-	-	1.2	0.265	250	[138]
2017	M57	TFC membrane	SPEEK blended PSf support, PA active layer	Phase inversion, interfacial polymerization	DI water (0.5 M NaCl)	22.4 ± 2.1	3.1	2.16 ± 0.13	191 ± 47	[79]
2017	M58	TFC membrane	PVDF vertically oriented porous substrates (VOPs), PA layer	Bidirectional freezing process, interfacial polymerization	DI water (1 M NaCl)	70.3	7.8	4.71 ± 0.22	99.1 ± 3.7	[12]

(continued)

Table 1 Continued

Year	Designation	Membranes	Materials	Preparation	Draw solution (DS)	Water flux in FO mode (LMFH)	RSF (gMH)	Intrinsic parameters			Ref.
								A (LMFH/bar)	B (LMH)	S ( $\mu\text{m}$ )	
2017	M59	Dual-layered nanocomposite membrane	PSf/GO substrate, PA active layer	Phase inversion, interfacial polymerization	DI water (1 M NaCl)	33.8	6.42	1.46	0.25	130	[69]
2017	M60	LBL membrane	PDA modified PVDF substrate, SA/PEI selective layer	Phase inversion, layer-by-layer	–	–	–	1.27 $\pm$ 0.06	0.03 $\pm$ 0.01	–	[44]
2017	M61	TFN membrane	INTs-incorporated PSf substrate, PA active layer	Phase inversion, interfacial polymerization	DI water (1 M NaCl)	7.5 $\pm$ 2.5	12 $\pm$ 1	3.03 $\pm$ 0.08	2.92 $\pm$ 0.29	2090	[94]
2017	M62	Polyvinyl chloride and layered double hydroxide composite membrane	PVC/LDH substrate, PA active layer	Phase inversion, interfacial polymerization	DI water (1 M NaCl)	37.46 $\pm$ 0.85	3.57 $\pm$ 0.2	3.61 $\pm$ 0.019	0.1816 $\pm$ 0.033	303	[18]
2017	M63	LbL assembled membrane	SPES support layer, chitosan/GO selective layer	Phase inversion, layer-by-layer	DI water (1 M Na <sub>2</sub> SO <sub>4</sub> )	24 $\pm$ 0.5	2.5	2.95	0.45	–	[139]
2017	M64	Chitosan-based active layer membrane	SPES-PES support layer, chitosan thin active layer	Phase inversion, interfacial polymerization	DI water (1 M NaCl)	18 $\pm$ 1.5	11 $\pm$ 1	2.87	0.72	–	[140]
2017	M65	TFC membrane	Polyketone support layer, PA active layer	Phase inversion, interfacial polymerization	DI water (0.6 M NaCl)	30.3 $\pm$ 0.5	0.078 $\pm$ 0.012 (mol/m <sup>2</sup> h)	2.79 $\pm$ 0.05	0.54 $\pm$ 0.02	176 $\pm$ 4	[87]
2017	M66	TFC membrane	PVDF/PFSA substrate, PA selective layer	Phase inversion, interfacial polymerization	DI water (1 M NaCl)	27 $\pm$ 3.75	8 $\pm$ 2.5	2.97 $\pm$ 0.06	0.39 $\pm$ 0.13	334.6 $\pm$ 3.5	[141]

2017	M67	TFN membrane	ZnO nanoparticles-incorporated PVDF substrate, PA active layer	Phase inversion, interfacial polymerization	–	–	0.75	0.26	413	[142]
2018	M68	pH-responsive TFC membrane	CPES-PES asymmetric support layer, PA active layer	Non-solvent induced phase inversion via immersion precipitation method, interfacial polymerization	DI water (1 M NaCl)	14.23 (pH = 3) 20 (pH = 7) 28 (pH = 12)	5.31 ± 0.09	5.61 ± 0.06	653.94	[81]
2018	M69	ST-modified TFC membrane	PES support layer, ST functionalized PA active layer	Non-solvent induced phase inversion, interfacial polymerization, chemical modification of the membrane surface with functional materials of sodium taurine	DI water, (0.5 M MgCl <sub>2</sub> ) DI water, (1 M MgCl <sub>2</sub> ) DI water, (2 M MgCl <sub>2</sub> )	14.7 ± 0.9 20 ± 0.8 26.7	0.82 ± 0.1	0.069 ± 0.002	–	[143]
2018	M70	TFC membrane	Commercial TFC membrane, PDA coating	PDA coating performed under moderate shaking for 0.5 h on a commercial TFC membrane	10 mM NaCl (1 M NaCl)	9 ± 0.9	2.2	2 (LMH)	1250	[95]
2018	M71	Aquaporin hollow fiber membrane	Aquaporin proteins incorporated into the active layer	–	ED (1 M NaCl)	13.2	0.43	0.05	210	[102]

(continued)

Table 1 Continued

Year	Designation	Membranes	Materials	Preparation	Draw solution (DS)	Water flux in FO mode (LMFH)	RSF (gMH)	Intrinsic parameters			Ref.
								A (LMFH/bar)	B (LMH)	S ( $\mu\text{m}$ )	
2018	M72	PVA-modified TFC membrane	PVA coated PVDF nanofiber support layer, PA active layer	Electrospinning, PVA dip coating catalyze crosslinking, interfacial polymerization	ED (0.5 M NaCl) ED (1 M NaCl) DI water (1.5 M NaCl) ED (1.5 M NaCl)	24.9 ~34 ~40 ~50	3.3 4.7 5.4 6.7	2.1	0.22	154	[55]
2018	M73	NTFC membrane	PS/PAN nanofiber support, PA active layer	Electrospinning, interfacial polymerization	DI water (1 M NaCl)	38.3 PRO mode	10.1 PRO mode	3.68 $\pm$ 0.23	0.32 $\pm$ 0.12	340	[100]
2018	M74	PVDF-CA TFC membrane	PVDF-CA dual composite nanofiber support, PA active layer	Coaxial electrospinning dual support, interfacial polymerization	DI water (0.5 M NaCl) DI water (1 M NaCl)	31.3 35	0.8 1	2.79	0.07	190	[89]
2018	M75	Support free symmetric PTAODH membrane	PTAODH polymer	Solvent evaporation method	DI water (1 M NaSO <sub>4</sub> )	3.5 (15 $\mu\text{m}$ ) 8 (8 $\mu\text{m}$ ) 11.8 (5 $\mu\text{m}$ )	1 (15 $\mu\text{m}$ ) 3 (8 $\mu\text{m}$ ) 5 (5 $\mu\text{m}$ )	0.16	0.039	~0	[63]
2018	M76	DSA-2Na TFC membrane	PES support layer, DSA-2Na modified PA active layer	Induced phase inversion, interfacial polymerization, chemical modification	DI water (0.5 M NaCl)	12.6 $\pm$ 0.9	1.6 $\pm$ 0.3	0.71 $\pm$ 0.2	0.094 $\pm$ 0.05	–	[61]
2018	M77	TFC membrane	PES support layer, PA active layer, zwitterion silver nanoparticles	Non-solvent induced phase separation method, interfacial polymerization, zwitterion silver nanoparticles surface modification	DI water (1 M NaCl)	15	7.5	1.166	0.14	–	[144]

2018	M78	TFC-PA-CNT membrane	PES support layer, CNT interlayer, PA active layer	Commercial PES, CNT spray coating, interfacial polymerization	DI water (1 M NaCl) DI water (0.5 M NaCl) DI water (1.5 M NaCl) DI water (2 M NaCl)	30 18 37.5 40	– – – –	2 ± 0.2	0.05 ± 0.01	197 ± 15	[145]
2018	M79	TFC-PRh membrane	PES support layer, PRh-NPs incorporated PA active layer	Commercial PES, PRh-NPs incorporation during interfacial polymerization	DI water (1 M NaCl) DI water (1.5 M NaCl)	31 41	100 mmol/m <sup>2</sup> h 115 mmol/m <sup>2</sup> h	1.6 ± 0.1	0.22 ± 0.01	128 ± 2	[146]
2018	M80	PVDF-LBL TFC membrane	PVDF nanofibers support layer, PEI-PAA polyelectrolyte layer, PA active layer	Electrospun PVDF, PAA and PEI polyelectrolyte LBL deposition, interfacial polymerization	DI water (0.5 M NaCl) DI water (1 M NaCl)	24.1 31	2.8 4	4.12	0.38	221	[78]
2019	M81	Reduced graphene oxide/carbon nanotube hollow fiber membrane	CNT hollow fiber substrate, RGO active layer	Wet-spinning method coupling with a pyrolysis process, electrophoretic deposition method	DI water (1 M NaCl)	–	–	2.11	0.051	202	[83]
2019	M82	Polyacrylonitrile-supported FO membranes	PAN support layer, PA active layer	Phase inversion, interfacial polymerization with HCl washing	DI water (1 M NaCl)	34.2	5.81	3.26 ± 0.14	0.2079 ± 0.03	387	[53]
2019	M83	TFN membrane	Layered double hydroxides (LDHs)-incorporated PSf support layer, PA active layer	Phase inversion, interfacial polymerization with HCl washing	DI water (1 M NaCl)	20.1	4.2	7.29 ± 0.31	3.63 ± 0.69	668.58 ± 50.55	[147]

(continued)

Table 1 Continued

Year	Designation	Membranes	Materials	Preparation	Draw solution (DS)	Water flux in FO mode (LMH)	RSF (g/MH)	Intrinsic parameters			Ref.
								A (LMH/bar)	B (LMH)	S ( $\mu\text{m}$ )	
2019	M84	Plasma functionalized hydroxyapatite (Hapf) incorporated TFN-FO membrane	CA/Hapf support layer, Hapf/PA active layer	Phase inversion, interfacial polymerization	DI water (1 M NaCl)	22.6 $\pm$ 0.5	13.5 $\pm$ 0.5	1.41 ( $\pm$ 0.03)	1.62 ( $\pm$ 0.08)	865	[96]
2019	M85	Novel graphene quantum dots (GQDs)-incorporated thin film composite (TFC) membranes	PAN support layer, GQDs-incorporated PA active layer	Interfacial polymerization on PAN commercial UF membrane	DI water (0.5 M MgCl <sub>2</sub> )	12.9	1.41	2.547 $\pm$ 0.010	0.19 $\pm$ 0.02	781.6	[148]
2019	M86	Hollow fiber thin-film composite membranes	PES support layer, PA coating layer	Dry-jet spinning, vacuum-assisted interfacial polymerization (VAIP) technique	DI water (1 M NaCl)	30 $\pm$ 1	4.2	2.26	0.28	190	[149]
2019	M87	Aquaporin-incorporated membrane	PSf support layer, PA active layer containing aquaporin	Phase inversion, interfacial polymerization	DI water (1 M NaCl)	22.82	3.82	0.87	0.12	188	[56]

2020	M88	TFC PSf-g-PDMA FO membrane	PSf graft poly(2-dimethylaminoethylmethacrylate) (PSf-g-PDMA) support layer, PA active layer	Phase inversion, interfacial polymerization	DI water (1 M NaCl)	~5	2.5	2.05 ± 0.09	0.61 ± 0.08	546.5 ± 44	[64]
2020	M89	Ceramic based FO membrane	Mullite ceramic substrate, TiO <sub>2</sub> /CNT interlayers, PA active layer	Dry-wet spinning, interfacial polymerization	DI water (1 M NaCl)	~18	~5	2 ± 0.1	0.58 ± 0.03	248 ± 20	[16]
2020	M90	Sandwich-like SWCNTs-coated TFC FO membrane	CNT-PES-CNT, PA active layer	MF commercial membrane, CNT coating, interfacial polymerization	DI water (1 M NaCl)	18.1	1.11	1.59 ± 0.02	0.1 ± 0.01	324.42 ± 34	[150]

process [20]; which is true in this case as DI water is used as FS. A rigorous comparison of each studied membrane is carried out on the basis of productivity and selectivity. Selectivity is evaluated through the *B/A* ratio; the lower this ratio is, the more selective the membrane is expected to be [62]. This ratio, expressed in units of pressure, can be considered as the effective osmotic pressure loss caused by the reverse diffusion of draw solutes [77].

This procedure was followed for all membranes using reported intrinsic parameters given in Table 1. Integral LbL membranes were not selected in this study except for the M80 membrane as it shows high NaCl retention [78]. These membranes generally show low selectivity to monovalent ions such as NaCl due to their solute rejection mechanism governed by the Donnan effect [62]. LbL membranes are usually tested using multivalent solutes such as MgCl<sub>2</sub>, explaining the lack of available data related to their permeability to NaCl.

#### 4. Results and discussion

Table 3 lists predicted water fluxes for various FO membranes collected from the literature (Table 1), as well as their selectivity. These membranes have been classified based on their productivity (water flux) as primary criterion, with selectivity as the secondary criterion. This makes it possible to consider all the parameters affecting membranes performances, thus easing identification of desired properties for different FO applications. In applications such as water treatment or desalination for example, high water flux can be preferred, while the selectivity criterion can be preferential in applications where a high rejection rate is critical (pharmaceutical, food industry, biomedical, etc.). High water flux and selectivity are generally both significant performance indicators, but a compromise must be reached depending on the targeted application.

The FO membranes presented in Table 3 can be categorized into sulfonated membranes (PES, PSf), cellulosic membranes (CA, CTA, CE), PVDF membranes, PAN membranes and polyketone membranes. These materials are usually associated to other polymers such as sulfonated poly(ether ether ketone) (SPEEK) [79], sulfonated poly(phenylene oxide) (SPPO) [80], carboxylic polyethersulfone (CPES) [81] and others, or incorporate diverse other materials (such as TiO<sub>2</sub> [57,82], SiO<sub>2</sub> [13,59], Zn<sub>2</sub>Ge nanowire [35], carbon nanotubes (CNTs) [19,83], graphene oxide GO [67,84,85]) to constitute the support layer. To a lesser extent, materials such as plastic [18] and ceramics [16] have also been used as substrates for FO membranes fabrication.

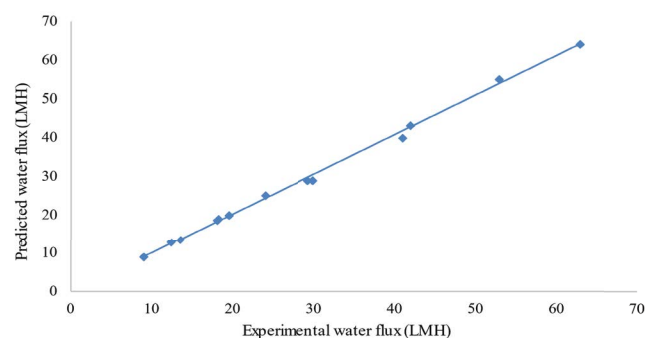


Fig. 3. Comparison of predicted and experimental water flux.

Table 2  
Model predictions and experimental water flux data relative error

Membranes	Feed and draw solutions testing conditions	Average experimental water flux (LMH)	Error (%)	Ref.
Oasys-TFC	DI water, 1.05 M NaCl	24	4.17	[20]
PA/PAN-eTFC	DI water, 0.5 M NaCl	18.2	4.40	
PA/PAN-eTFC	DI water, 1 M NaCl	29.33	1.13	[72]
PA/PAN-eTFC	DI water, 2 M NaCl	41	2.44	
HTI-CTA	DI water, 1 M NaCl	9	0.67	
HTI-CTA	DI water, 1 M NaCl	13.5	1.48	[73,74]
TFC-FO	DI water, 1 M NaCl	18	2.78	
CTA-FO	DI water, 1 M NaCl	12.5	3.20	[71]
PSF-TFC	DI water, 0.5 M NaCl	19.5	2.56	
PSF-TFC	DI water, 1 M NaCl	30	3.33	
PSF-TFC	DI water, 2 M NaCl	42	2.38	[70]
PSF-TFC	DI water, 3 M NaCl	53	3.77	
PSF-TFC	DI water, 4 M NaCl	63	1.59	

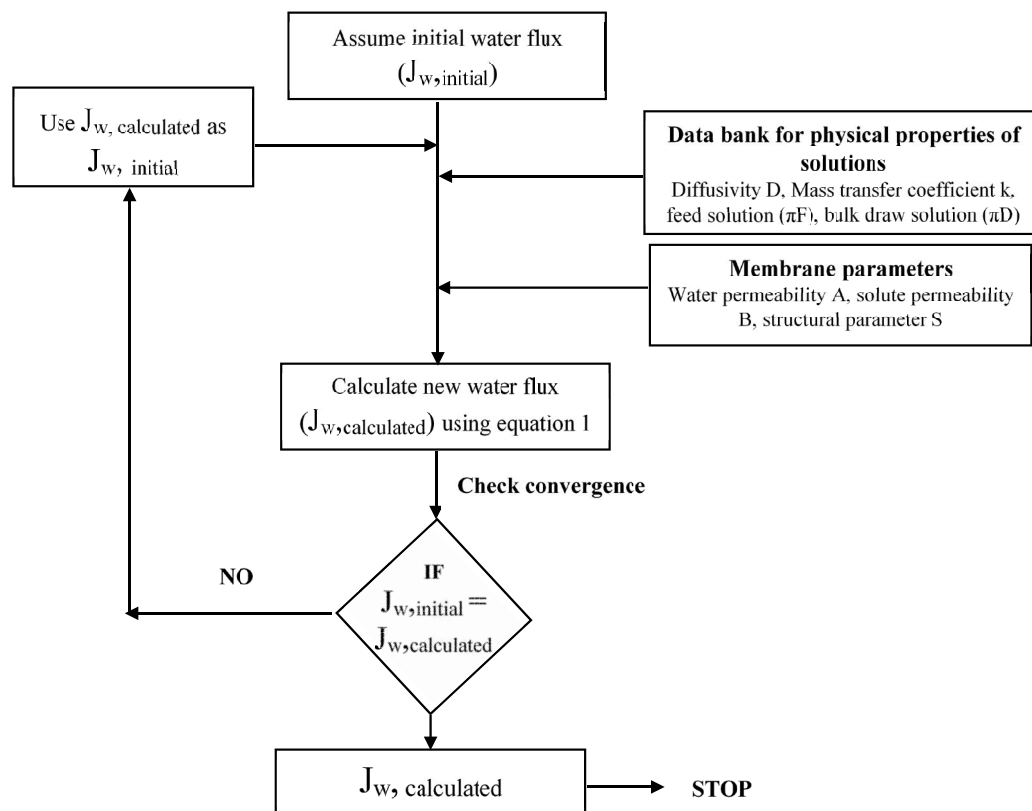


Fig. 4. FO model resolution algorithm.

About 53% of the studied membranes are made from sulfonated materials of which 30% are PSf and 23% are PES, with an average water flux of 23.33 and 22.96 LMH, respectively. PVDF-based membranes represent 14% and exhibit the highest average water flux at 30.81 LMH. Cellulosic and PAN-based membranes each represent 7% of the studied membranes, having an average water flux of 18.48 and 23.3 LMH respectively. Polyketone

membranes have an average water flux of 28.16 LMH and represent about 5% of the membranes studied. Result analysis and classification are given below.

#### 4.1. Highest performing FO membranes

The six membranes with the highest productivity are shown in Fig. 5, namely, M53, M48, M80, M65, M72 and

Table 3  
Predicted water flux of studied FO membranes

Memb.	$J_w$ (LMH)	Selectivity (bar)	Memb.	$J_w$ (LMH)	Selectivity (bar)	Memb.	$J_w$ (LMH)	Selectivity (bar)
M61	6.650	0.964	M12	19.621	0.064	M36	29.446	0.207
M70	9.191	0.909	M88	19.910	0.138	M62	29.548	0.050
M84	10.400	1.149	M83	20.400	0.498	M38	29.718	0.073
M50	12.539	0.744	M56	20.650	0.221	M29	29.830	0.208
M67	12.672	0.347	M26	21.82	0.832	M78	29.968	0.025
M71	13.280	0.116	M19	22.414	0.091	M81	30.290	0.024
M14	13.703	0.200	M33	24.032	0.393	M59	31.300	0.171
M85	13.990	0.075	M47	24.268	0.195	M57	31.536	0.074
M15	14.099	0.342	M18	24.576	0.190	M31	31.550	0.177
M46	14.680	0.126	M82	24.680	0.077	M86	32.210	0.124
M39	15.440	0.448	M28	25.363	0.298	M44	32.293	0.269
M34	15.642	3.400	M24	26.039	0.038	M79	33.150	0.138
M11	15.988	0.091	M25	26.255	0.740	M37	33.388	0.092
M23	16.857	0.325	M66	26.310	0.131	M72	34.861	0.105
M43	17.044	0.357	M45	26.960	0.072	M74	35.460	0.025
M49	17.480	0.443	M51	27.281	0.169	M65	36.880	0.194
M68	18.480	1.056	M73	27.579	0.087	M80	37.800	0.092
M27	19.088	0.194	M55	28.389	1.156	M48	38.9	0.137
M87	19.450	0.110	M35	28.636	0.108	M53	48.835	0.650

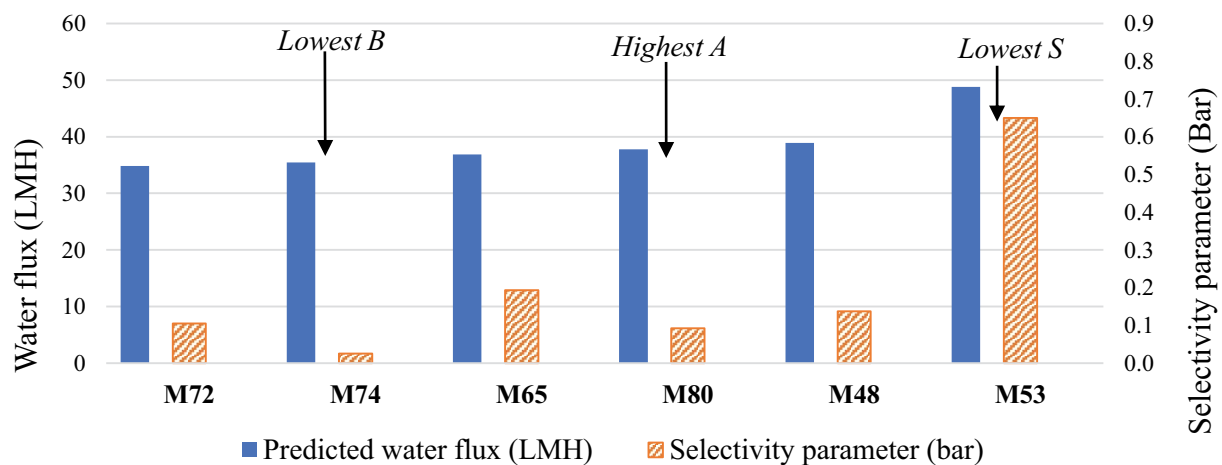


Fig. 5. FO membranes with highest predicted water flux and their selectivity indicators ( $B/A$ ).

M74 membranes. The highest water flux at 48.83 LMH is obtained by the M53 membrane. This may be ascribed to its small structural parameter of 29.7  $\mu\text{m}$ , the lowest  $S$  value obtained in the study. This low structural parameter is in fact attributed to a very low tortuosity that significantly reduces ICP effects, hence enabling very high-water flux. The M53 PVDF nanofiber substrate incorporates  $\text{SiO}_2$  nanoparticles, which improve the membrane's hydrophilicity, thereby achieving good water permeability. The membrane's selective layer is made of PA by interfacial polymerization. The high  $B/A$  ratio of the M53 membrane (0.65 Bar) indicates a reduced selectivity as shown in Fig. 5. Obaid et al. [59] reported a measured specific RSF of 0.67 bar using 1 M NaCl and DI water as DS and FS,

respectively. M48 [86] is a thin film nanocomposite (TFN) membrane with silica nanoparticles embedded in the polyetherimide (PEI) matrix as substrate and a PA active layer. The membrane shows high predicted water flux of 38.9 LMH. Integration of silica in the nanofibrous substrate led to increased porosity (83% for 1.6 wt.% of silica loading) and pore size. The reduced structural parameter and nanofibrous interconnected macropores morphology resulted in ICP mitigation and enhanced water flux. The M48 membrane has also a low selectivity indicator of 0.137 bar that suggests a high rejection rate. The M80, M65, M74 and M72 membranes have estimated water fluxes of 37.8, 36.88, 35.46 and 34.861 LMH, respectively. The M80 [78] is a TFC membrane with a PVDF nanofiber support layer coated

with PAA and a selective double-layer constituted of a PEI/PAA layer formed by the layer-by-layer deposition method on which a PA layer is deposited by IP. In contrast with other LbL membranes, M80 has a higher NaCl rejection rate (96.46%) than that of the HTI's TFC membrane [78]. This is due to its selective barrier consisting of a PA layer and a PAA/PEI layer. This membrane has also a high water permeability coefficient of 4.12 LMH/bar owing to the presence of the PAA/PEI layer, which has improved the hydrophilicity of the membrane. Nevertheless, the LbL preparation method can be expensive, which could hinder the industrialization and large-scale production of such membranes. The M65 membrane consists of a polyketone support layer made by phase inversion (NIPS) and a PA active formed by IP [87]. This membrane has interesting intrinsic properties: a relatively high permeability of 2.79 LMH bar<sup>-1</sup>, low structural parameter and solute permeability of 176 μm and 0.54 LMH, respectively. Its relatively low *B/A* ratio (0.194 bar) also suggests a good membrane selectivity. The structure of support layer obtained by NIPS with small surface pores is favourable for hosting a PA layer [88]. M74 [89] and M72 [55] membranes are TFC membranes with nanofibers substrates. M74 support layer is made of PVDF/CA produced by coaxial electrospinning, which consists in covering the hydrophobic PVDF with hydrophilic CA, thus producing a dual layer composite nanofiber substrate. TFC membranes having coaxial electrospun PVDF/CA substrates possess superior performances compared with the PVDF electrospun substrate as shown in the study by Shibuya et al. [89]. The structure of the PVDF/CA nanofibrous substrate is also favourable for ICP effects mitigation. The M74 membrane has excellent selectivity with a *B/A* ratio of 0.025, the lowest among the membranes studied. Its specific RSF of 0.03 g L<sup>-1</sup> is by far the lowest value reported in the literature [89]. The M72 membrane has also a support layer made of PVDF nanofibers coated with a hydrophilic PVA layer, which explains its good water permeability. M72 also presents good selectivity with a *B/A* ratio of 0.104 bar.

Although the M53 membrane has shown the highest water productivity, its poor selectivity can represent a serious weakness in specific applications such as in pharmaceutical or food industry where it becomes an important criterion. Poor selectivity has also a significant impact on the economic feasibility of the process as it affects replenishment costs, a critical factor in establishing OPEX costs [90–92]. The M80 and M74 membranes could, therefore, be considered as better candidate as they associate high water flux to high selectivity. But as LBL fabrication method (M80) is still expensive [11], this could impede its industrial development and commercialization. The membrane M74 composed of PVDF-core/CA-sheath composite nanofibers exhibits the lowest *B/A* among all studied membranes. Its hydrophilic CA-sheath with small surface pore size is favourable for the formation of a highly cross-linked PA layer, hence the high selectivity.

Results have shown that nanofiber TFC membranes exhibit the highest performance in terms of water fluxes; among the six highest-productivity membranes, four have nanofiber support layers. Electrospun membranes generally have low structural parameters due to their open,

porous and non-tortuous structure. Their use in FO processes, therefore, reduces ICP effects [72], which represent one of the main limitations for FO membranes. Since the degree of ICP is dependent on the structure of the membrane support layer, it is crucial to design membranes with reduced structural parameters. Electrospun supports may, however, be subject to low mechanical strength [72] explaining why they are still in the R&D stage. A compromise is thus required between selectivity, structural parameter and mechanical strength of membranes [93]. The *S* parameter is a function of membranes tortuosity, porosity and thickness [11,20]. It can be reduced either by decreasing the tortuosity or thickness, or by increasing porosity of the support layer. Reducing the thickness or increasing the porosity of the support layer (which would reduce its density) may, however, result in a reduced membrane mechanical strength. The porosity and thickness of a membrane must, therefore, be optimized to provide the ability to simultaneously withstand the operating conditions while minimizing ICP effects. The mechanical behavior of the material must be taken into account; the better the mechanical behavior of the material is, the better the mechanical strength of the membrane is. Porosity and tortuosity can be controlled through the manufacturing process. While membranes prepared by electrospinning often have low tortuosity, phase-inversion membranes exhibit a “finger-like pore” structure when phase separation occurs instantaneously and a “sponge-like pore” structure for delayed phase separation. The scaffold-like structure of nanofibers and the finger-like pore structure are less tortuous and more favourable to reduce ICP, hence to achieve high productivity.

#### 4.2. Least performing FO membranes

The three least performing membranes are the M61, M70 and M84, with respective water fluxes of 6.65, 9.191 and 10.4 LMH. A comparison of predicted water fluxes and selectivity parameters of these membranes is presented in Fig. 7. The M61 [94] membrane is a TFN membrane having a PSf support layer incorporated with imogolite nanotubes and a PA active layer. Despite a high *A* parameter (3.03 LMH bar<sup>-1</sup>), the membrane shows poor water flux mainly due to its very high structural parameter of 2,090 μm, giving rise to high ICP effects. Compared with the M65 membrane [87] (176 μm and 2.79 LMH bar<sup>-1</sup>), the M61 has a structural parameter of about 12 times higher for a similar water permeability coefficient. Thickness and porosity of M61 ( $\epsilon = 76.4\%$ ,  $t = 64.2 \mu\text{m}$ ) being similar to those of M65 ( $\epsilon = 84.5\%$ ,  $t = 82.7 \mu\text{m}$ ), the M61 membrane, therefore, presents a very high tortuosity estimated at 13.89, which is approximately 14 times higher than that of M65. This high tortuosity can explain its high structural parameter, thus resulting in high ICP effects. The low selectivity of the M61 membrane, shown by a *B/A* ratio of 0.9637 bar could result in high RSF, which may exacerbate ICP effects and further impact the FO water flux.

As shown in the SEM image (Fig. 6) [59,94], the M61 top layer has a sponge-like pore structure known for substrates with high tortuosity, which explains the high structural parameter of the membrane. On the other hand, the SEM image of the M53 membrane, which has the lowest

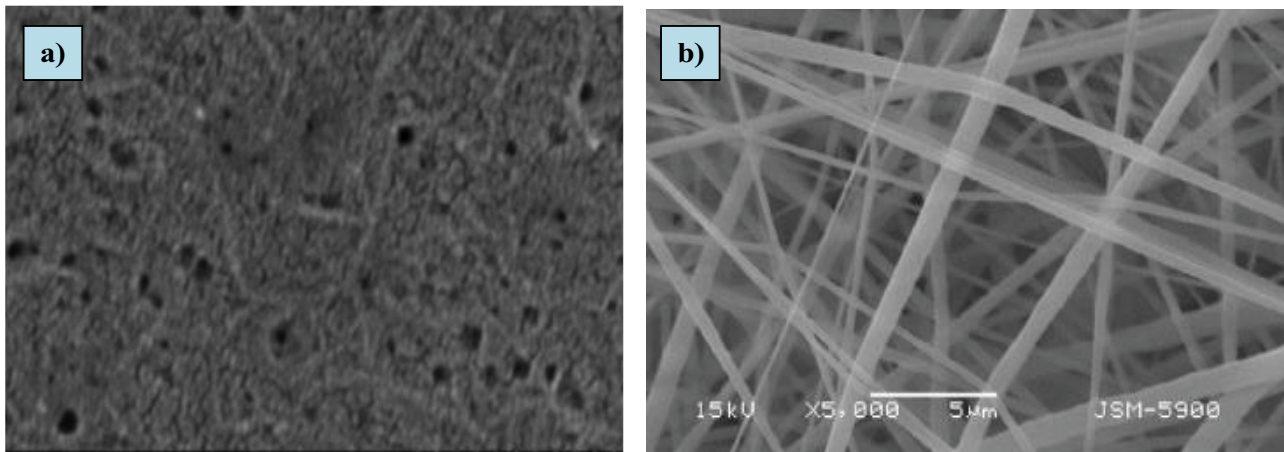


Fig. 6. SEM images of membranes substrates: (a) M61 membrane [94] and (b) M53 membrane [59].

S parameter of all the studied membranes shows scaffold-like pore structure, with low tortuosity and high surface porosity.

The M70 [95] and M84 [96] membranes are, respectively, a commercial TFC membrane coated with a PDA layer, and a TFN membrane composed of a CA substrate with a PA selective layer integrating functionalized hydroxyapatite. These two membranes also show high structural parameters, with respective to values of 1,250 and 865 μm. The water permeability parameter of both membranes being comparable with other studied membranes, their low water fluxes can, therefore, be attributed to the high structural parameters. The lack of data related to the tortuosity, porosity and thickness of these membranes do not allow for more in-depth analysis.

4.3. Classification and analysis of the other studied membranes

All membranes that weren't previously identified as best or worst performer can be classified by water flux

values into a low-to-medium flux (12.5 to 22.5 LMH) category and a high flux (24 to 34 LMH) category. Fig. 8a illustrates the calculated water fluxes, with the center zone being the low-to-medium flux range and the outer colored zone corresponding to the high water flux range. Membrane selectivity, while not the primary selection parameter for performances, is illustrated in Fig. 8b. In this case, higher selectivity is found at periphery and lower selectivity toward the center.

4.3.1. Low-to-medium water flux membranes

Low-to-medium water flux membranes exhibit values ranging from 12,539 LMH (M50) to 22,414 LMH (M19). The predominant membranes in this class are prepared by phase inversion mainly using PSf, PES, CA/CTA materials (M15, M14, M50, M40, M39, M34, M27, M88). Most of these membranes have a relatively high structural parameter, averaging 422.02 μm, which has a negative impact on the water flux. The calculated average water and solute

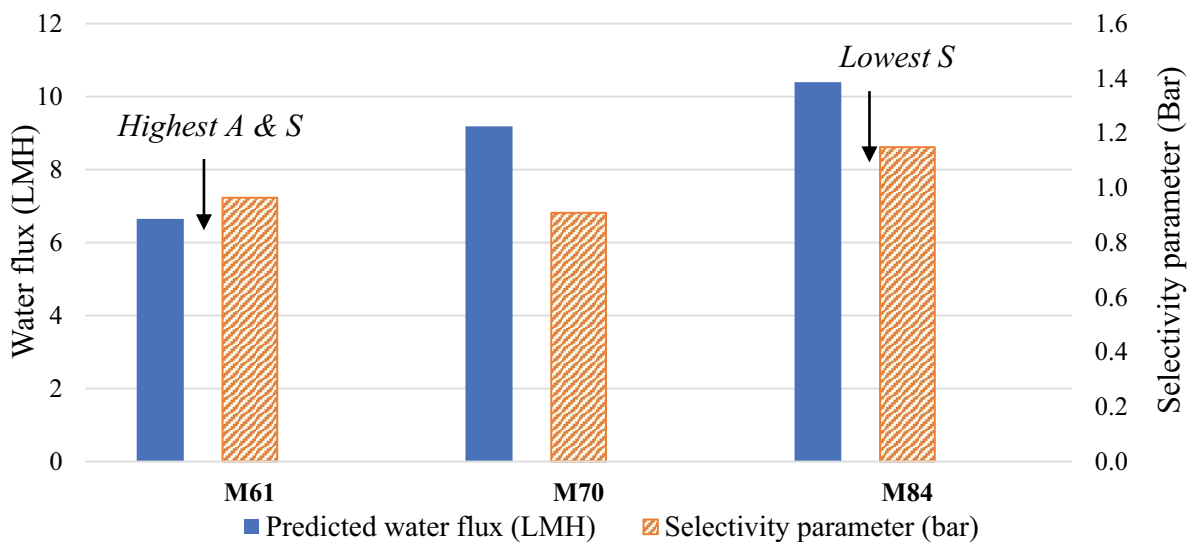


Fig. 7. FO membranes with lowest predicted water flux and their selectivity indicators (B/A).

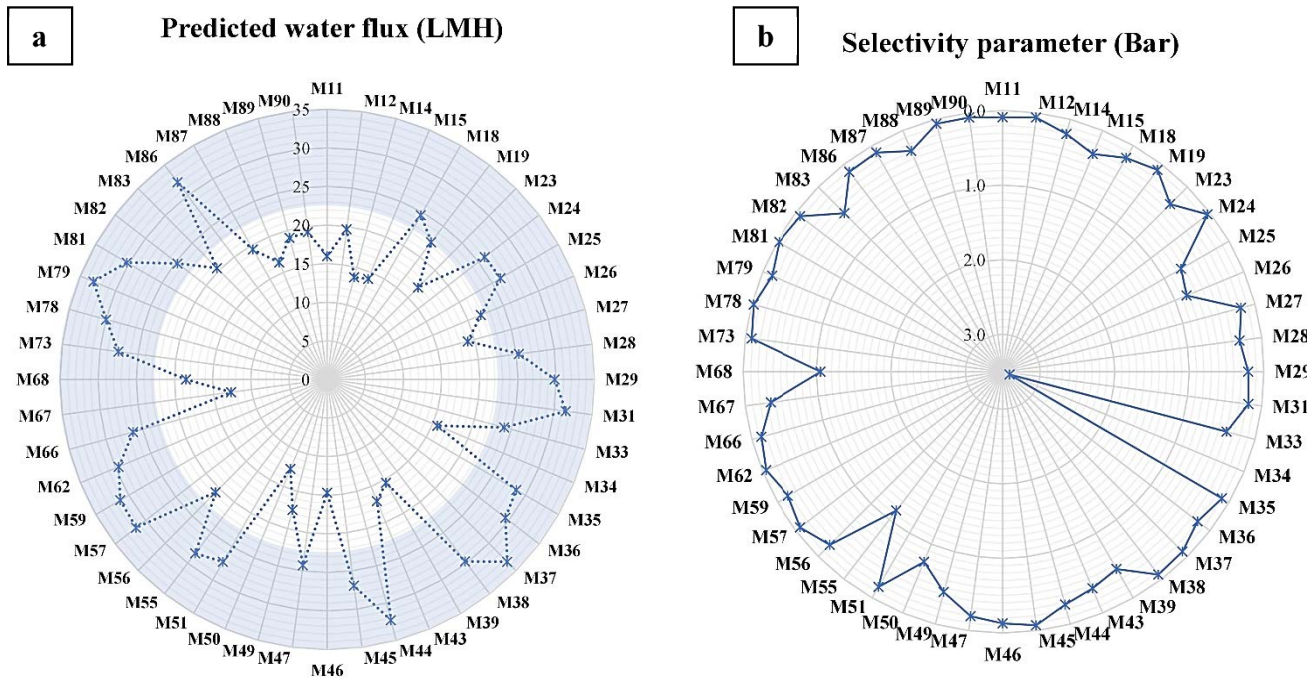


Fig. 8. Predicted water fluxes (a) and calculated selectivity indicators (b) of low-to-medium and high water flux membranes categories.

permeability coefficients  $A$  and  $B$  are  $2.021 \text{ LMH bar}^{-1}$  and  $1.22 \text{ LMH}$ , respectively.

The M83 and M68 membranes have the highest structural parameters of all membranes in this category, with respective values of  $668.5$  and  $653.9 \mu\text{m}$ , and should, therefore, have a lower water flux than the other membranes due to higher ICP effects. These two membranes have, however, the highest water permeability parameters among all studied membranes ( $7.29$  and  $5.31 \text{ LMH bar}^{-1}$ , respectively) that help ICP mitigation. In contrast, the M49 [84], M87 [56] and M19 [97] membranes have the lowest water permeability coefficients of this category ( $0.61$ ,  $0.73$  and  $0.75 \text{ LMH bar}^{-1}$ , respectively) but possess structural parameters ( $148$ ,  $153$  and  $107 \mu\text{m}$ , respectively) significantly lower than the calculated average, meaning lower ICP effects and thus enhanced water flux.

#### 4.3.2. High water flux membranes

Membranes with a water flux above  $22.5 \text{ LMH}$  are considered to have a high flux. These membranes consist of TFC mostly prepared by phase inversion or, to a lesser extent, by electrospinning. Many of these membranes, namely M26, M31, M35, M36, M51, M55, M62 and M66, are made from PSf or PES nanoparticles (NPs) integrated support layers and a PA selective layer. Different types of NPs are used, including  $\text{TiO}_2$  [82], silica ( $\text{SiO}_2$ ) [34], GO [98], LDH [18], etc. A few membranes, such as M24 and M28, consist however of PSf support layers and active layers incorporating functionalized CNTs NPs [99] and silica NPs [58], respectively. The presence of NPs into the active layer enhances the membrane's hydrophilicity and a better crosslinking of the PA layer.

Other approaches for support layers preparation have been investigated, among which are the blending of two polymers [79,80,100], dual-layered substrate [69] or dual-selective layers [101] have been investigated. The support layers of M29 [80], M57 [79] and M73 [100] membranes have thus been prepared by blending PSf with hydrophilic polymers. The M59 [69] substrate is instead a dual layered PSf/GO nanosheets fabricated by a double blade casting technique to form a bottom structure with high porosity and a dense top layer to allow a better PA layer deposition. The M29 substrate is made from a polymer blend of PSf/SPPO prepared by phase inversion, on top of which a PA active layer was deposited by IP. It is a TFC membrane with internal generation of osmotic pressure by immobilization of counter ions ( $\text{Na}^+$ ) in the SPPO, which helps attenuate the osmotic gradient reduction due to ICP phenomena. The M57 support layer consists of a PSf/SPEEK blend prepared by phase inversion via co-casting. This approach yielded an improved porosity due to an open pore structure at the bottom surface of the support layer, hence reducing the membrane structural parameter. The enhanced hydrophilicity and reduced  $S$  parameter lead to higher water fluxes. The M73 membrane consists of a PA layer deposited by IP on an electrospun polymeric blend of PSf/PAN nanofibers. Membranes with high water flux have an average a structural parameter of  $250.06 \mu\text{m}$ , a water permeability coefficient of  $2.45 \text{ LMH bar}^{-1}$  and a solute permeability coefficient  $B$  of  $0.549 \text{ LMH}$ .

The water flux of a membrane is mainly determined by its structural parameter and water permeability coefficient. From the low-to-medium water flux to the high water flux membranes, it can be noted that the average structural parameter has decreased by  $\sim 41\%$  while the average

A-parameter has only slightly increased (+17.5%). It can be, therefore, concluded that the observed increase in water flux is more related to a significant reduction of the mean structural parameter rather than an increase of the A parameter. Regarding membranes selectivity, a decrease of 55% has been noticed between the two categories, which indicates a better overall selectivity of the high water flux category membranes. Considering that a high RSF contributes to the accentuation of CP phenomena and thus a reduced water permeation, selectivity also distinguishes membranes from the low and high water flux categories.

#### 4.4. Commercial FO membranes

After Oasys Water commercialized, the first TFC membrane designed specifically for FO applications, development of FO membranes has gained a renewed interest leading to the creation of new companies. Available data from commercial FO membranes have been collected and their water flux predicted under the same conditions as those used for R&D membranes. This allows for a fair comparison with the best R&D FO membranes identified in this study. Membranes selectivity of commercial FO has also been evaluated through the  $B/A$  ratio.

The commercial FO membranes reported in Table 4 are either CTA- or TFC-based membranes. They are supplied by Fluid Technology Solutions (FTS), previously Hydration Technology Innovation (HTI), Porifera, Toyobo, Oasys Water and Aquaporin A/S. Aquaporin Inside™ hollow fiber are TFC membranes integrated with biomimetic aquaporin proteins into the PA active layer that act as “water channels” [102]. Various membrane module configurations are commercialized, including spiral wound modules using flat-sheet membranes (FTS, Oasys Water and Porifera) and hollow fibers modules (HF) (Toyobo and Aquaporin).

As shown in Table 4 and reported by other studies [32,103], the Porifera membrane shows the highest water flux compared with other commercial membranes, followed by the Oasys Water and HTI TFC membranes. Generally, TFC membranes tend to perform better than CTA membranes as they have demonstrated reduced water permeance. In addition to a restricted pH and temperature operating range [11,71,104], cellulosic membranes are also subjected to hydrolysis, which severely impacts their

performance. These limitations make TFC membranes the most commonly used in FO.

#### 4.5. From R&D to commercial production

R&D membranes clearly show better water flux and selectivity than commercial membranes as shown in Fig. 9. While a real progress has been made in commercial TFC membranes for FO process, more development is required to improve their performance. The structure (porosity, tortuosity, thickness) of the support layer, materialized through its structural parameter, is generally the limiting factor of performance for membranes [93]. To the best of our knowledge, commercial membrane substrates are manufactured using a phase inversion process, leading to a tortuous structure with sponge-like pores, which may exacerbate the effects of ICP [93,107]. It is, therefore, necessary to develop new approaches for the preparation of TFC-FO membranes substrates.

Among the possible development pathways, the first is on the efficient use of electrospinning for the preparation of substrates with low tortuosity [59,108,109]. The second pathway is on developing an appropriate fabrication process using hydrophilic materials that can yield self-supported membranes with the mechanical strength required to operate in FO process. This would remove the reinforcing layer currently used in commercial membranes to increase their mechanical strength, but has the side-effect of increasing mass transfer resistance. The third area of development is on the active polyamide layer that, while exhibiting a good solute rejection rate, is susceptible to chlorine attack and fouling because of its surface chemical structure [110]. The aromatic PA layer obtained by polymerization of the MPD and TMC monomers is well known for its “ridge-and-valley” structure, which significantly promotes fouling [37,110,111] while a smooth surface would minimize fouling. To mitigate this fouling issue, some researchers have proposed to deposit an anti-fouling layer on the PA layer [112,113] while others are trying to improve its hydrophilicity through incorporation of hydrophilic nanomaterials [33,114,115], but progress is still needed.

The lab-to-industry transition is, however, subject to a number of conditions [32,93,116] making the launch of a new membrane a very challenging process especially

Table 4  
Commercial FO membranes, intrinsic membranes parameters, predicted water flux and calculated selectivity parameter

Membranes	A (LMH/bar)	B (LMH)	S ( $\mu\text{m}$ )	Predicted water flux (LMH)	Selectivity parameter (Bar)	Ref.
Oasys Water	1.94	1.99	274	24.02	1.025	[105]
HTI-CTA	0.51	2.19	600	8.076	4.29	[105]
HTI-TFC	1.63	1.42	295	21.46	0.871	[105]
Aquaporin	0.43	0.05	210	12.358	0.116	[102]
Toyobo HF-A	0.27	0.08	1024	4.83	0.296	[102]
Toyobo HF-B	0.29	0.02	724	5.948	0.068	[102]
Toyobo HF-C	0.55	0.04	639	8.749	0.072	[102]
Porifera	2.2	0.576	215	29.657	0.261	[103]
FTS CTA	0.69	0.34	707	9.092	0.492	[106]
FTS HTI	1.25	0.19	471	14.906	0.152	[106]

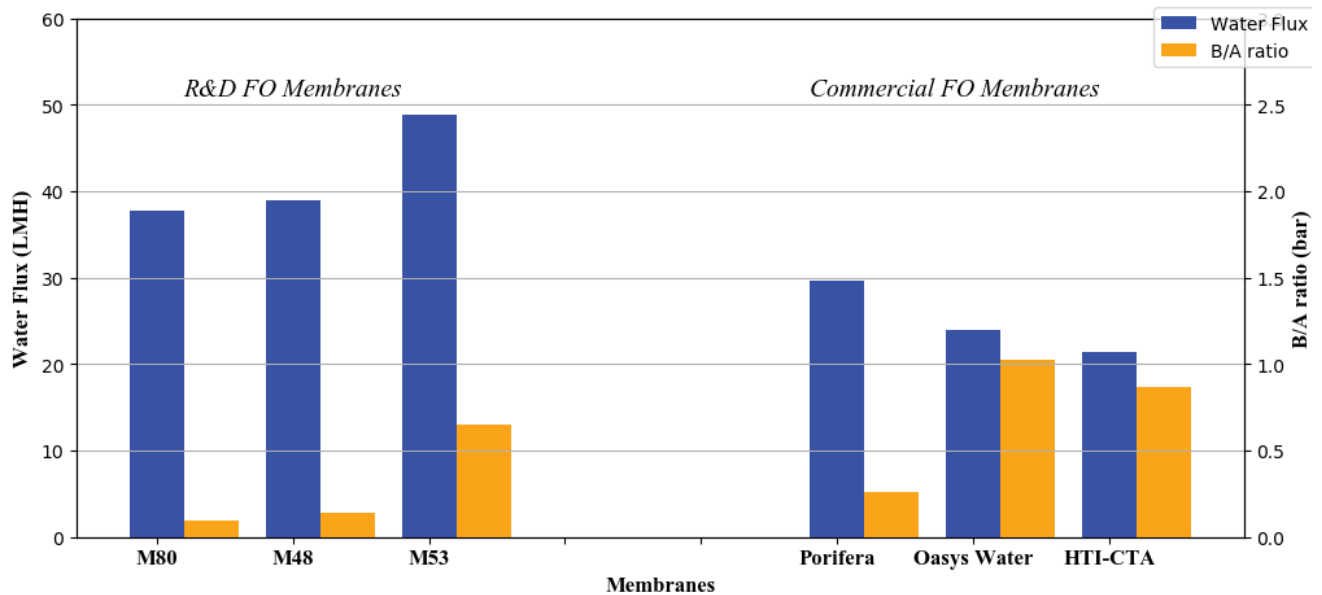


Fig. 9. Best performing R&D vs. commercial FO membranes.

when the technology is still in its infancy. For an innovative membrane to enter the market, extensive testing is required where the membrane is subjected to every possible operating condition to simulate realistic operation in various FO applications. In addition to high water flux and selectivity, high mechanical and chemical stability must be proven as well as compatibility with a wide range of chemicals/draw agents. Ease of fabrication, availability of used materials, reproducibility and cost production considerations are crucial to achieve industrialization and commercialization. To succeed scaling-up, the long-term performances and stability must be proven through pilot testing. The next generation of FO membranes should consider these criteria and be designed with available and low-cost materials to reduce manufacturing costs and enable the laboratory-to-industry transition.

## 5. Conclusion

In this work performances of various R&D and commercial FO membranes were evaluated, using water flux as primary criterion. The water flux of each membrane was predicted using a model to standardize both operating and thermodynamic conditions, thus allowing a fair comparison of performances and subsequent classification of membranes. Membrane selectivity was calculated via the  $B/A$  ratio.

FO membranes are mainly prepared from sulfonated- (PES, PSf), cellulosic- (CA, CTA, CE), PVDF-, PAN- or polyketone-based materials. Half of the membranes studied were composed of sulfonated materials, yielding relatively high water fluxes. The best performances were, however, achieved with PVDF-based membranes.

This study has shown that nanofiber-based PVDF membranes constitute an interesting candidate for future FO membranes development as they represent four of the six best performing membranes and only 14% of the studied membranes. Thus, efforts to improve next generation of

commercial FO membranes should be focused on three main axes:

- Fabrication process: optimization of preparation techniques, to design low ICP membranes with excellent mechanical properties, which will prevent the need for a reinforcement layer.
- Materials: use more hydrophilic materials to replace hydrophobic substrate materials as PSF, PES usually employed in TFC membranes.
- Selective layer: modification of the active layer to form low fouling propensity, chemically stable and high-selectivity TFC selective layer.

Finally cost considerations and ease of fabrication need to be taken into account to lower market entry barriers.

## Acknowledgements

The authors would like to thank IRESEN, the Research Institute for Solar Energy and New Energies for the continuing funding.

## References

- [1] UNESCO, The United Nations World Water Development Report 2019: Leaving No One Behind, 75352 Paris 07 SP, France, 2019.
- [2] R.W. Hofste, P. Reig, L. Schleifer, 17 Countries, Home to One-Quarter of the World's Population, Face Extremely High Water Stress, World Resour. Inst. (2019) N/A. <https://www.wri.org/print/65485>.
- [3] M.W. Shahzad, M. Burhan, L. Ang, K.C. Ng, Energy-water-environment nexus underpinning future desalination sustainability, *Desalination*, 413 (2017) 52–64.
- [4] D. Zarzo, D. Prats, Desalination and energy consumption. What can we expect in the near future?, *Desalination*, 427 (2018) 1–9.
- [5] I. Ndiaye, S. Vaudreuil, T. Bounahmidi, Forward osmosis process: state-of-the-art of membranes, *Sep. Purif. Rev.*, 50 (2019) 1–21.

- [6] I. Chaoui, S. Abderafi, S. Vaudreuil, T. Bounahmidi, Water desalination by forward osmosis: draw solutes and recovery methods—review, *Environ. Technol. Rev.*, 8 (2019) 25–46.
- [7] C. Klaysom, T.Y. Cath, T. Depuydt, I.F.J. Vankelecom, Forward and pressure retarded osmosis: potential solutions for global challenges in energy and water supply, *Chem. Soc. Rev.*, 42 (2013) 6959–6989.
- [8] S.S. Manickam, J.R. McCutcheon, Understanding mass transfer through asymmetric membranes during forward osmosis: a historical perspective and critical review on measuring structural parameter with semi-empirical models and characterization approaches, *Desalination*, 421 (2017) 110–126.
- [9] T.Y. Cath, A.E. Childress, M. Elimelech, Forward osmosis: principles, applications, and recent developments, *J. Membr. Sci.*, 281 (2006) 70–87.
- [10] T.S. Chung, S. Zhang, K.Y. Wang, J. Su, M.M. Ling, Forward osmosis processes: yesterday, today and tomorrow, *Desalination*, 287 (2012) 78–81.
- [11] M. Qasim, N.A. Darwish, S. Sarp, N. Hilal, Water desalination by forward (direct) osmosis phenomenon: a comprehensive review, *Desalination*, 374 (2015) 47–69.
- [12] H.Q. Liang, W.S. Hung, H.H. Yu, C.C. Hu, K.R. Lee, J.Y. Lai, Z.K. Xu, Forward osmosis membranes with unprecedented water flux, *J. Membr. Sci.*, 529 (2017) 47–54.
- [13] M. Rastgar, A. Shakeri, A. Bozorg, H. Salehi, V. Saadattalab, Impact of nanoparticles surface characteristics on pore structure and performance of forward osmosis membranes, *Desalination*, 421 (2017) 179–189.
- [14] W. Suwaileh, N. Pathak, H. Shon, N. Hilal, Forward osmosis membranes and processes : a comprehensive review of research trends and future outlook, *Desalination*, 485 (2020) 114455. <https://doi.org/10.1016/j.desal.2020.114455>.
- [15] Y. Yu, Q.Y. Wu, H.Q. Liang, L. Gu, Z.K. Xu, Novel thin film composite membranes supported by cellulose triacetate porous substrates for high-performance forward osmosis, *J. Membr. Sci.*, 492 (2015) 209–219.
- [16] M. Zhang, W. Jin, F. Yang, M. Duke, Y. Dong, C.Y. Tang, Engineering a Nanocomposite Interlayer for a Novel Ceramic-Based Forward Osmosis Membrane with Enhanced Performance, *Environ. Sci. Technol.*, 54 (2020) 7715–7724.
- [17] X. Zhao, J. Li, C. Liu, A novel TFC-type FO membrane with inserted sublayer of carbon nanotube networks exhibiting the improved separation performance, *Desalination*, 413 (2017) 176–183.
- [18] P.M. Pardeshi, A.K. Mungray, A.A. Mungray, Polyvinyl chloride and layered double hydroxide composite as a novel substrate material for the forward osmosis membrane, *Desalination*, 421 (2017) 149–159.
- [19] M. Tian, Y.N. Wang, R. Wang, Synthesis and characterization of novel high-performance TFN FO membranes with nanofibrous substrate reinforced by functionalized carbon nanotubes, *Desalination*, 370 (2015) 79–86.
- [20] A. Tiraferri, N.Y. Yip, A.P. Straub, S. Romero-Vargas Castrillon, M. Elimelech, A method for the simultaneous determination of transport and structural parameters of forward osmosis membranes, *J. Membr. Sci.* 444 (2013) 523–538.
- [21] Y. Wang, K. Goh, X. Li, L. Setiawan, R. Wang, Membranes and processes for forward osmosis-based desalination: Recent advances and future prospects, *Desalination*, 434 (2018) 81–99.
- [22] W.A. Suwaileh, D.J. Johnson, S. Sarp, N. Hilal, Advances in forward osmosis membranes: Altering the sub-layer structure via recent fabrication and chemical modification approaches, *Desalination*, 436 (2018) 176–201.
- [23] Y. Cai, X.M. Hu, A critical review on draw solutes development for forward osmosis, *Desalination*, 391 (2016) 16–29.
- [24] D.J. Johnson, W.A. Suwaileh, A.W. Mohammed, N. Hilal, Osmotic's potential: An overview of draw solutes for forward osmosis, *Desalination*, 434 (2018) 100–120.
- [25] S. Loeb, Production of energy from concentrated brines by pressure-retarded osmosis. I. Preliminary technical and economic correlations, *J. Membr. Sci.* 1 (1976) 49–63.
- [26] S. LOEB, S., SOURIRAJAN, High Flow Porous Membranes For Separating Water From Saline Solutions, 1964.
- [27] M.C. Porter, Handbook of Industrial Membrane Technology, Westwood, New Jersey, U.S.A., 1990.
- [28] S. Zhang, K.Y. Wang, T.S. Chung, H. Chen, Y.C. Jean, G. Amy, Well-constructed cellulose acetate membranes for forward osmosis: minimized internal concentration polarization with an ultra-thin selective layer, *J. Membr. Sci.*, 360 (2010) 522–535.
- [29] W.A. Phillip, J.D. Schiffman, M. Elimelech, High performance thin-film membrane, *Environ. Sci. Technol.*, 44 (2010) 3812–3818.
- [30] J.R. McCutcheon, R.L. McGinnis, M. Elimelech, A novel ammonia-carbon dioxide forward (direct) osmosis desalination process, *Desalination*, 174 (2005) 1–11.
- [31] Oasys Water Inc., Oasys Water commercialises FO membrane technology, *Membr. Technol.*, 2010 (2010) 1–16.
- [32] A.M. Awad, R. Jalab, J. Minier-Matar, S. Adham, W.S. Nasser, S.J. Judd, The status of forward osmosis technology implementation, *Desalination*, 461 (2019) 10–21.
- [33] A. Tiraferri, Y. Kang, E.P. Giannelis, M. Elimelech, Highly hydrophilic thin-film composite forward osmosis membranes functionalized with surface-tailored nanoparticles, *ACS Appl. Mater. Interfaces*, 4 (2012) 5044–5053.
- [34] X. Liu, H.Y. Ng, Fabrication of layered silica-polysulfone mixed matrix substrate membrane for enhancing performance of thin-film composite forward osmosis membrane, *J. Membr. Sci.*, 481 (2015) 148–163.
- [35] Z.X. Low, Q. Liu, E. Shamsaei, X. Zhang, H. Wang, Preparation and characterization of thin-film composite membrane with nanowire-modified support for forward osmosis process, *Membranes (Basel)*, 5 (2015) 136–149.
- [36] Y. Yu, Q.Y. Wu, H.Q. Liang, L. Gu, Z.K. Xu, Preparation and characterization of cellulose triacetate membranes via thermally induced phase separation, *J. Appl. Polym. Sci.*, 134 (2017) 1–10.
- [37] Q.Y. Wu, X.Y. Xing, Y. Yu, L. Gu, Z.K. Xu, Novel thin film composite membranes supported by cellulose triacetate porous substrates for high-performance forward osmosis, *Polymer (Guildf)*, 153 (2018) 150–160.
- [38] N.N. Bui, M.L. Lind, E.M. V Hoek, J.R. McCutcheon, Electrospun nanofiber supported thin film composite membranes for engineered osmosis, *J. Membr. Sci.*, 385–386 (2011) 10–19.
- [39] M. Tian, C. Qiu, Y. Liao, S. Chou, R. Wang, Preparation of polyamide thin film composite forward osmosis membranes using electrospun polyvinylidene fluoride (PVDF) nanofibers as substrates, *Sep. Purif. Technol.*, 118 (2013) 727–736.
- [40] L. Huang, J.T. Arena, J.R. McCutcheon, Author's Accepted Manuscript Surface Modified PVDF Nanofiber Supported Thin Film Composite Membranes for Forward Osmosis, (2015). <https://doi.org/10.1016/j.memsci.2015.10.030>.
- [41] W. Xie, G.M. Geise, B.D. Freeman, H.S. Lee, G. Byun, J.E. McGrath, Polyamide interfacial composite membranes prepared from m-phenylene diamine, trimesoyl chloride and a new disulfonated diamine, *J. Membr. Sci.*, 403–404 (2012) 152–161.
- [42] R. Wang, L. Shi, C.Y. Tang, S. Chou, C. Qiu, A.G. Fane, Characterization of novel forward osmosis hollow fiber membranes, *J. Membr. Sci.*, 355 (2010) 158–167.
- [43] J.Y. Lee, S. Qi, X. Liu, Y. Li, F. Huo, C.Y. Tang, Synthesis and characterization of silica gel-polyacrylonitrile mixed matrix forward osmosis membranes based on layer-by-layer assembly, *Sep. Purif. Technol.*, 124 (2014) 207–216.
- [44] C. Liu, X. Lei, L. Wang, J. Jia, X. Liang, X. Zhao, H. Zhu, Investigation on the removal performances of heavy metal ions with the layer-by-layer assembled forward osmosis membranes, *Chem. Eng. J.*, 327 (2017) 60–70.
- [45] K.Y. Wang, T.S. Chung, J.J. Qin, Polybenzimidazole (PBI) nanofiltration hollow fiber membranes applied in forward osmosis process, *J. Membr. Sci.*, 300 (2007) 6–12.
- [46] K.Y. Wang, Q. Yang, T.S. Chung, R. Rajagopalan, Enhanced forward osmosis from chemically modified polybenzimidazole (PBI) nanofiltration hollow fiber membranes with a thin wall, *Chem. Eng. Sci.*, 64 (2009) 1577–1584.
- [47] Q. Yang, K.Y. Wang, T.S. Chung, Dual-layer hollow fibers with enhanced flux as novel forward osmosis membranes for water production, *Environ. Sci. Technol.*, 43 (2009) 2800–2805.

- [48] K.Y. Wang, R.C. Ong, T.S. Chung, Double-skinned forward osmosis membranes for reducing internal concentration polarization within the porous sublayer, *Ind. Eng. Chem. Res.*, 49 (2010) 4824–4831.
- [49] S. Zhang, K.Y. Wang, T.S. Chung, Y.C. Jean, H. Chen, Molecular design of the cellulose ester-based forward osmosis membranes for desalination, *Chem. Eng. Sci.*, 66 (2011) 2008–2018.
- [50] J. Su, Q. Yang, J.F. Teo, T. Chung, Cellulose acetate nanofiltration hollow fiber membranes for forward osmosis processes, *J. Membr. Sci.*, 355 (2010) 36–44.
- [51] M. Sairam, E. Sereewatthanawut, K. Li, A. Bismarck, A.G. Livingston, Method for the preparation of cellulose acetate flat sheet composite membranes for forward osmosis-Desalination using  $MgSO_4$  draw solution, *Desalination*, 273 (2011) 299–307.
- [52] R.C. Ong, T.S. Chung, B.J. Helmer, J.S. De Wit, Novel cellulose esters for forward osmosis membranes, *Ind. Eng. Chem. Res.*, 51 (2012) 16135–16145.
- [53] H.E. Kwon, S.J. Kwon, S.J. Park, M.G. Shin, S.H. Park, M.S. Park, H. Park, J.H. Lee, High performance polyacrylonitrile-supported forward osmosis membranes prepared via aromatic solvent-based interfacial polymerization, *Sep. Purif. Technol.*, 212 (2019) 449–457.
- [54] L. Huang, J.T. Arena, J.R. McCutcheon, Surface modified PVDF nanofiber supported thin film composite membranes for forward osmosis, *J. Membr. Sci.*, 499 (2016) 352–360.
- [55] M.J. Park, R.R. Gonzales, A. Abdel-Wahab, S. Phuntsho, H.K. Shon, Hydrophilic polyvinyl alcohol coating on hydrophobic electrospun nanofiber membrane for high performance thin film composite forward osmosis membrane, *Desalination*, 426 (2018) 50–59.
- [56] Z. Liang, Y. Yun, M. Wang, G. Liu, P. Lu, W. Yang, C. Li, Performance evaluation of interfacial polymerisation-fabricated aquaporin-based biomimetic membranes in forward osmosis, *RSC Adv.*, 9 (2019) 10715–10726.
- [57] D. Emadzadeh, W.J. Lau, T. Matsuura, M. Rahbari-Sisakht, A.F. Ismail, A novel thin film composite forward osmosis membrane prepared from  $PSf-TiO_2$  nanocomposite substrate for water desalination, *Chem. Eng. J.*, 237 (2014) 70–80.
- [58] N. Niksefat, M. Jahanshahi, A. Rahimpour, The effect of  $SiO_2$  nanoparticles on morphology and performance of thin film composite membranes for forward osmosis application, *Desalination*, 343 (2014) 140–146.
- [59] M. Obaid, Z.K. Ghouri, O.A. Fadali, K.A. Khalil, A.A. Almajid, N.A.M. Barakat, Amorphous  $SiO_2$  NP-incorporated poly(vinylidene fluoride) electrospun nanofiber membrane for high flux forward osmosis desalination, *ACS Appl. Mater. Interfaces*, 8 (2016) 4561–4574.
- [60] M. Ghanbari, D. Emadzadeh, W.J. Lau, S.O. Lai, T. Matsuura, A.F. Ismail, Synthesis and characterization of novel thin film nanocomposite (TFN) membranes embedded with halloysite nanotubes (HNTs) for water desalination, *Desalination*, 358 (2015) 33–41.
- [61] T. Ni, Q. Ge, Highly hydrophilic thin-film composition forward osmosis (FO) membranes functionalized with aniline sulfonate/bisulfonate for desalination, *J. Membr. Sci.*, 564 (2018) 732–741.
- [62] S. Qi, W. Li, Y. Zhao, N. Ma, J. Wei, T.W. Chin, C.Y. Tang, Influence of the properties of layer-by-layer active layers on forward osmosis performance, *J. Membr. Sci.*, 423–424 (2012) 536–542.
- [63] M. Li, V. Karanikola, X. Zhang, L. Wang, M. Elimelech, A self-standing, support-free membrane for forward osmosis with no internal concentration polarization, *Environ. Sci. Technol. Lett.*, 5 (2018) 266–271.
- [64] H. Salehi, A. Shakeri, H. Mahdavi, R.G.H. Lammertink, Improved performance of thin-film composite forward osmosis membrane with click modified polysulfone substrate, *Desalination*, 496 (2020) 114731. <https://doi.org/10.1016/j.desal.2020.114731>.
- [65] K.L. Lee, R.W. Baker, H.K. Lonsdale, Membranes for power generation by pressure-retarded osmosis, *J. Membr. Sci.*, 8 (1981) 141–171.
- [66] J.R. McCutcheon, M. Elimelech, Influence of concentrative and dilutive internal concentration polarization on flux behavior in forward osmosis, *J. Membr. Sci.*, 284 (2006) 237–247.
- [67] N.Y. Yip, A. Tiraferri, W.A. Phillip, J.D. Schiffman, L.A. Hoover, Y.C. Kim, M. Elimelech, Thin-film composite pressure retarded osmosis membranes for sustainable power generation from salinity gradients, *Environ. Sci. Technol.*, 45 (2011) 4360–4369.
- [68] A. Achilli, T.Y. Cath, A.E. Childress, Power generation with pressure retarded osmosis: an experimental and theoretical investigation, *J. Membr. Sci.*, 343 (2009) 42–52.
- [69] S. Lim, M.J. Park, S. Phuntsho, L.D. Tijing, G.M. Nisola, W.G. Shim, W.J. Chung, H.K. Shon, Dual-layered nanocomposite substrate membrane based on polysulfone/graphene oxide for mitigating internal concentration polarization in forward osmosis, *Polymer (Guildf)*, 110 (2017) 36–48.
- [70] P. Xiao, L.D. Nghiem, Y. Yin, X.M. Li, M. Zhang, G. Chen, J. Song, T. He, A sacrificial-layer approach to fabricate polysulfone support for forward osmosis thin-film composite membranes with reduced internal concentration polarisation, *J. Membr. Sci.*, 481 (2015) 106–114.
- [71] C. Boo, Y.F. Khalil, M. Elimelech, Performance evaluation of trimethylamine-carbon dioxide thermolytic draw solution for engineered osmosis, *J. Membr. Sci.*, 473 (2015) 302–309.
- [72] S.F. Pan, Y. Dong, Y.M. Zheng, L. Bin Zhong, Z.H. Yuan, Self-sustained hydrophilic nanofiber thin film composite forward osmosis membranes: preparation, characterization and application for simulated antibiotic wastewater treatment, *J. Membr. Sci.*, 523 (2017) 205–215.
- [73] W.A. Phillip, J.S. Yong, M. Elimelech, Reverse draw solute permeation in forward osmosis: modeling and experiments, *Environ. Sci. Technol.*, 44 (2010) 5170–5176.
- [74] C. Suh, S. Lee, Modeling reverse draw solute flux in forward osmosis with external concentration polarization in both sides of the draw and feed solution, *J. Membr. Sci.*, 427 (2013) 365–374.
- [75] K. Madsen, H.B. Nielsen, O. Tingleff, *Methods For Non-Linear Least Squares Problems (2nd ed.)*, Informatics and Mathematical Modelling Technical University of Denmark, Richard Petersens Plads, Buildings 321, DK-2800 Kgs. Lyngby, 2004, p. 60.
- [76] L. Chekli, S. Phuntsho, H.K. Shon, S. Vigneswaran, J. Kandasamy, A. Chanan, A review of draw solutes in forward osmosis process and their use in modern applications, *Desal. Water Treat.*, 43 (2012) 167–184.
- [77] W.C.L. Lay, J. Zhang, C. Tang, R. Wang, Y. Liu, A.G. Fane, Analysis of salt accumulation in a forward osmosis system, *Sep. Sci. Technol.*, 47 (2012) 1837–1848.
- [78] R.R. Gonzales, M.J. Park, L. Tijing, D.S. Han, S. Phuntsho, H.K. Shon, Modification of nanofiber support layer for thin film composite forward osmosis membranes via layer-by-layer polyelectrolyte deposition, *Membranes (Basel)*, 8 (2018) 1–15.
- [79] G. Chen, R. Liu, H.K. Shon, Y. Wang, J. Song, X.M. Li, T. He, Open porous hydrophilic supported thin-film composite forward osmosis membrane via co-casting for treatment of high-salinity wastewater, *Desalination*, 405 (2017) 76–84.
- [80] Z. Zhou, J.Y. Lee, T.S. Chung, Thin film composite forward-osmosis membranes with enhanced internal osmotic pressure for internal concentration polarization reduction, *Chem. Eng. J.*, 249 (2014) 236–245.
- [81] H. Salehi, A. Shakeri, M. Rastgar, Carboxylic polyethersulfone: a novel pH-responsive modifier in support layer of forward osmosis membrane, *J. Membr. Sci.*, 548 (2018) 641–653.
- [82] D. Emadzadeh, W.J. Lau, T. Matsuura, A.F. Ismail, M. Rahbari-Sisakht, Synthesis and characterization of thin film nanocomposite forward osmosis membrane with hydrophilic nanocomposite support to reduce internal concentration polarization, *J. Membr. Sci.*, 449 (2014) 74–85.
- [83] X. Fan, Y. Liu, X. Quan, A novel reduced graphene oxide/carbon nanotube hollow fiber membrane with high forward osmosis performance, *Desalination*, (2019) 451 117–124.
- [84] P. Lu, S. Liang, L. Qiu, Y. Gao, Q. Wang, Thin film nanocomposite forward osmosis membranes based on layered double

- hydroxide nanoparticles blended substrates, *J. Membr. Sci.*, 504 (2016) 196–205.
- [85] D. Emadzadeh, W.J. Lau, M. Rahbari-Sisakht, H. Ilbeygi, D. Rana, T. Matsuura, A.F. Ismail, Synthesis, modification and optimization of titanate nanotubes-polyamide thin film nanocomposite (TFN) membrane for forward osmosis (FO) application, *Chem. Eng. J.*, 281 (2015) 243–251.
- [86] M. Tian, Y.N. Wang, R. Wang, A.G. Fane, Synthesis and characterization of thin film nanocomposite forward osmosis membranes supported by silica nanoparticle incorporated nanofibrous substrate, *Desalination*, 401 (2017) 142–150.
- [87] M. Yasukawa, S. Mishima, Y. Tanaka, T. Takahashi, H. Matsuyama, Thin-film composite forward osmosis membrane with high water flux and high pressure resistance using a thicker void-free polyketone porous support, *Desalination*, 402 (2017) 1–9.
- [88] A.K. Ghosh, E.M.V. Hoek, Impacts of support membrane structure and chemistry on polyamide-polysulfone interfacial composite membranes, *J. Membr. Sci.*, 336 (2009) 140–148.
- [89] M. Shibuya, M.J. Park, S. Lim, S. Phuntsho, H. Matsuyama, H.K. Shon, Novel CA/PVDF nanofiber supports strategically designed via coaxial electrospinning for high performance thin-film composite forward osmosis membranes for desalination, *Desalination*, 445 (2018) 63–74.
- [90] A. Achilli, T.Y. Cath, A.E. Childress, Selection of inorganic-based draw solutions for forward osmosis applications, *J. Membr. Sci.*, 364 (2010) 233–241.
- [91] Y. Choi, H. Cho, Y. Shin, Y. Jang, S. Lee, Economic evaluation of a hybrid desalination system combining forward and reverse osmosis, *Membranes (Basel)*, 6 (2015). <https://doi.org/10.3390/membranes6010003>.
- [92] G. Blandin, A.R.D. Verliefde, C.Y. Tang, P. Le-Clech, Opportunities to reach economic sustainability in forward osmosis-reverse osmosis hybrids for seawater desalination, *Desalination*, 363 (2015) 26–36.
- [93] L. Xia, M.F. Andersen, C. Hélix-Nielsen, J.R. McCutcheon, Novel commercial aquaporin flat-sheet membrane for forward osmosis, *Ind. Eng. Chem. Res.*, 56 (2017) 11919–11925.
- [94] Y.H. Pan, Q.Y. Zhao, L. Gu, Q.Y. Wu, Thin film nanocomposite membranes based on imoligite nanotubes blended substrates for forward osmosis desalination, *Desalination*, 421 (2017) 160–168.
- [95] H. Guo, Z. Yao, J. Wang, Z. Yang, X. Ma, C.Y. Tang, Polydopamine coating on a thin film composite forward osmosis membrane for enhanced mass transport and antifouling performance, *J. Membr. Sci.*, 551 (2018) 234–242.
- [96] A.L. Ohland, V.M.M. Salim, C.P. Borges, Nanocomposite membranes for osmotic processes: incorporation of functionalized hydroxyapatite in porous substrate and in selective layer, *Desalination*, 463 (2019) 23–31.
- [97] G. Han, T.S. Chung, M. Toriida, S. Tamai, Thin-film composite forward osmosis membranes with novel hydrophilic supports for desalination, *J. Membr. Sci.*, 423–424 (2012) 543–555.
- [98] Y. Kim, J.H. Lee, Y.C. Kim, K.H. Lee, I.S. Park, S.J. Park, Operation and simulation of pilot-scale forward osmosis desalination with ammonium bicarbonate, *Chem. Eng. Res. Des.*, 94 (2015) 390–395.
- [99] M. Amini, M. Jahanshahi, A. Rahimpour, Synthesis of novel thin film nanocomposite (TFN) forward osmosis membranes using functionalized multi-walled carbon nanotubes, *J. Membr. Sci.*, 435 (2013) 233–241.
- [100] S. Shokrollahzadeh, S. Tajik, Fabrication of thin film composite forward osmosis membrane using electrospun polysulfone/polyacrylonitrile blend nanofibers as porous substrate, *Desalination*, 425 (2018) 68–76.
- [101] R. Wei, S. Zhang, Y. Cui, R.C. Ong, T.S. Chung, B.J. Helmer, J.S. de Wit, Highly permeable forward osmosis (FO) membranes for high osmotic pressure but viscous draw solutes, *J. Membr. Sci.*, 496 (2015) 132–141.
- [102] J. Ren, J.R. McCutcheon, A new commercial biomimetic hollow fiber membrane for forward osmosis, *Desalination*, 442 (2018) 44–50.
- [103] P. Nasr, H. Sewilam, Investigating fertilizer drawn forward osmosis process for groundwater desalination for irrigation in Egypt, *Desal. Water Treat.*, 57 (2016) 26932–26942.
- [104] J.T. Arena, S.S. Manickam, K.K. Reimund, P. Brodskiy, J.R. McCutcheon, Characterization and performance relationships for a commercial thin film composite membrane in forward osmosis Desalination and Pressure Retarded Osmosis, *Ind. Eng. Chem. Res.*, 54 (2015) 11393–11403.
- [105] K.L. Hickenbottom, J. Vanneste, M. Elimelech, T.Y. Cath, Assessing the current state of commercially available membranes and spacers for energy production with pressure retarded osmosis, *Desalination*, 389 (2016) 108–118.
- [106] H.T. Madsen, S.S. Nissen, J. Muff, E.G. Søgaard, Pressure retarded osmosis from hypersaline solutions: investigating commercial FO membranes at high pressures, *Desalination*, 420 (2017) 183–190.
- [107] X. Song, Z. Liu, D.D. Sun, Nano gives the answer: Breaking the bottleneck of internal concentration polarization with a nanofiber composite forward osmosis membrane for a high water production rate, *Adv. Mater.*, 23 (2011) 3256–3260.
- [108] N.N. Bui, J.R. McCutcheon, Nanoparticle-embedded nanofibers in highly permselective thin-film nanocomposite membranes for forward osmosis, *J. Membr. Sci.*, 518 (2016) 338–346.
- [109] M. Obaid, H.O. Mohamed, A.S. Yasin, O.A. Fadali, K.A. Khalil, T. Kim, N.A.M. Barakat, A novel strategy for enhancing the electrospun PVDF support layer of thin-film composite forward osmosis membranes, *RSC Adv.*, 6 (2016) 102762–102772.
- [110] G.R. Xu, J.N. Wang, C.J. Li, Strategies for improving the performance of the polyamide thin film composite (PA-TFC) reverse osmosis (RO) membranes: surface modifications and nanoparticles incorporations, *Desalination*, 328 (2013) 83–100.
- [111] D.L. Shaffer, H. Jaramillo, S. Romero-Vargas Castrillón, X. Lu, M. Elimelech, Post-fabrication modification of forward osmosis membranes with a poly(ethylene glycol) block copolymer for improved organic fouling resistance, *J. Membr. Sci.*, 490 (2015) 209–219.
- [112] L. Shen, X. Zhang, J. Zuo, Y. Wang, Performance enhancement of TFC FO membranes with polyethyleneimine modification and post-treatment, *J. Membr. Sci.*, 534 (2017) 46–58.
- [113] Y. Wang, X. Li, C. Cheng, Y. He, J. Pan, T. Xu, Second interfacial polymerization on polyamide surface using aliphatic diamine with improved performance of TFC FO membranes, *J. Membr. Sci.*, 498 (2016) 30–38.
- [114] M. Mohammadifakhr, J. De Groot, A. Kemperman, E. Roesink, Forward osmosis: A critical review, *Processes*, 2020). <https://doi.org/10.3390/pr8040404>.
- [115] S.J. Shi, Y.H. Pan, S.F. Wang, Z.W. Dai, L. Gu, Q.Y. Wu, Aluminosilicate nanotubes embedded polyamide thin film nanocomposite forward osmosis membranes with simultaneous enhancement of water permeability and selectivity, *Polymers (Basel)*, 11 (2019). <https://doi.org/10.3390/polym11050879>.
- [116] M. Perry, S.U. Madsen, T. Jørgensen, S. Braekvelt, K. Lauritzen, C. Hélix-Nielsen, Challenges in commercializing biomimetic membranes, *Membranes (Basel)*, 5 (2015) 685–701.
- [117] S. Chou, L. Shi, R. Wang, C.Y. Tang, C. Qiu, A.G. Fane, Characteristics and potential applications of a novel forward osmosis hollow fiber membrane, *Desalination*, 261 (2010) 365–372.
- [118] J. Wei, C. Qiu, C.Y. Tang, R. Wang, A.G. Fane, Synthesis and characterization of flat-sheet thin film composite forward osmosis membranes, *J. Membr. Sci.*, 372 (2011) 292–302.
- [119] N. Widjojo, T.S. Chung, M. Weber, C. Maletzko, V. Warzelhan, The role of sulphonated polymer and macrovoid-free structure in the support layer for thin-film composite (TFC) forward osmosis (FO) membranes, *J. Membr. Sci.*, 383 (2011) 214–223.
- [120] Y. Yu, S. Seo, I.C. Kim, S. Lee, Nanoporous polyethersulfone (PES) membrane with enhanced flux applied in forward osmosis process, *J. Membr. Sci.*, 375 (2011) 63–68.

- [121] P. Sukitpaneevit, T.S. Chung, High performance thin-film composite forward osmosis hollow fiber membranes with macrovoid-free and highly porous structure for sustainable water production, *Environ. Sci. Technol.*, 46 (2012) 7358–7365.
- [122] N. Ma, J. Wei, R. Liao, C.Y. Tang, Zeolite-polyamide thin film nanocomposite membranes: Towards enhanced performance for forward osmosis, *J. Membr. Sci.*, 405–406 (2012) 149–157.
- [123] Y.H. Cho, J. Han, S. Han, M.D. Guiver, H.B. Park, Polyamide thin-film composite membranes based on carboxylated polysulfone microporous support membranes for forward osmosis, *J. Membr. Sci.*, 445 (2013) 220–227.
- [124] N. Widjojo, T.S. Chung, M. Weber, C. Maletzko, V. Warzelhan, A sulfonated polyphenylenesulfone (sPPSU) as the supporting substrate in thin film composite (TFC) membranes with enhanced performance for forward osmosis (FO), *Chem. Eng. J.*, 220 (2013) 15–23.
- [125] A. Soroush, W. Ma, Y. Silvino, M.S. Rahaman, Surface modification of thin film composite forward osmosis membrane by silver-decorated graphene-oxide nanosheets, *Environ. Sci. Nano*, 2 (2015) 395–405.
- [126] S.B. Kwon, J.S. Lee, S.J. Kwon, S.T. Yun, S. Lee, J.H. Lee, Molecular layer-by-layer assembled forward osmosis membranes, *J. Membr. Sci.*, 488 (2015) 111–120.
- [127] M.J. Park, S. Phuntsho, T. He, G.M. Nisola, L.D. Tijing, X.M. Li, G. Chen, W.J. Chung, H.K. Shon, Graphene oxide incorporated polysulfone substrate for the fabrication of flat-sheet thin-film composite forward osmosis membranes, *J. Membr. Sci.*, 493 (2015) 496–507.
- [128] Y. Wang, R. Ou, H. Wang, T. Xu, Graphene oxide modified graphitic carbon nitride as a modifier for thin film composite forward osmosis membrane, *J. Membr. Sci.*, 475 (2015) 281–289.
- [129] Z. Dabaghian, A. Rahimpour, Carboxylated carbon nanofibers as hydrophilic porous material to modification of cellulosic membranes for forward osmosis desalination, *Chem. Eng. Res. Des.*, 104 (2015) 647–657.
- [130] W. Fang, C. Liu, L. Shi, R. Wang, Composite forward osmosis hollow fiber membranes: Integration of RO- and NF-like selective layers for enhanced organic fouling resistance, *J. Membr. Sci.*, 492 (2015) 147–155.
- [131] R.C. Ong, T.S. Chung, J.S. de Wit, B.J. Helmer, Novel cellulose ester substrates for high performance flat-sheet thin-film composite (TFC) forward osmosis (FO) membranes, *J. Membr. Sci.*, 473 (2014) 63–71.
- [132] J. Ren, J.R. McCutcheon, Polyacrylonitrile supported thin film composite hollow fiber membranes for forward osmosis, *Desalination*, 372 (2015) 67–74.
- [133] M. Yasukawa, S. Mishima, M. Shibuya, D. Saeki, T. Takahashi, T. Miyoshi, H. Matsuyama, Preparation of a forward osmosis membrane using a highly porous polyketone microfiltration membrane as a novel support, *J. Membr. Sci.*, 487 (2015) 51–59.
- [134] A. Zirehpour, A. Rahimpour, F. Seyedpour, M. Jahanshahi, Developing new CTA/CA-based membrane containing hydrophilic nanoparticles to enhance the forward osmosis desalination, *Desalination*, 371 (2015) 46–57.
- [135] M. Ghanbari, D. Emadzadeh, W.J. Lau, H. Riazi, D. Almasi, A.F. Ismail, Minimizing structural parameter of thin film composite forward osmosis membranes using polysulfone/halloysite nanotubes as membrane substrates, *Desalination*, 377 (2016) 152–162.
- [136] X. Liu, S.L. Ong, H.Y. Ng, Fabrication of mesh-embedded double-skinned substrate membrane and enhancement of its surface hydrophilicity to improve anti-fouling performance of resultant thin-film composite forward osmosis membrane, *J. Membr. Sci.*, 511 (2016) 40–53.
- [137] X.Y. Chi, P.Y. Zhang, X.J. Guo, Z.L. Xu, A novel TFC forward osmosis (FO) membrane supported by polyimide (PI) microporous nanofiber membrane, *Appl. Surf. Sci.*, 427 (2018) 1–9.
- [138] M. Shibuya, M. Yasukawa, S. Mishima, Y. Tanaka, T. Takahashi, H. Matsuyama, A thin-film composite-hollow fiber forward osmosis membrane with a polyketone hollow fiber membrane as a support, *Desalination*, 402 (2017) 33–41.
- [139] H. Salehi, M. Rastgar, A. Shakeri, Anti-fouling and high water permeable forward osmosis membrane fabricated via layer by layer assembly of chitosan/graphene oxide, *Appl. Surf. Sci.*, 413 (2017) 99–108.
- [140] A. Shakeri, H. Salehi, M. Rastgar, Chitosan-based thin active layer membrane for forward osmosis desalination, *Carbohydr. Polym.*, 174 (2017) 658–668.
- [141] X. Zhang, L. Shen, W.Z. Lang, Y. Wang, Improved performance of thin-film composite membrane with PVDF/PFSA substrate for forward osmosis process, *J. Membr. Sci.*, 535 (2017) 188–199.
- [142] X. Zhao, J. Li, C. Liu, Improving the separation performance of the forward osmosis membrane based on the etched microstructure of the supporting layer, *Desalination*, 408 (2017) 102–109.
- [143] W. Xu, Q. Ge, Novel functionalized forward osmosis (FO) membranes for FO desalination: Improved process performance and fouling resistance, *J. Membr. Sci.*, 555 (2018) 507–516.
- [144] M. Qiu, C. He, Novel zwitterion-silver nanocomposite modified thin-film composite forward osmosis membrane with simultaneous improved water flux and biofouling resistance property, *Appl. Surf. Sci.*, 455 (2018) 492–501.
- [145] Z. Zhou, Y. Hu, C. Boo, Z. Liu, J. Li, L. Deng, X. An, High-performance thin-film composite membrane with an ultrathin spray-coated carbon nanotube interlayer, *Environ. Sci. Technol. Lett.*, 5 (2018) 243–248.
- [146] A. Rahimpour, S.F. Seyedpour, S. Aghapour Aktij, M. Dadashi Firouzjaei, A. Zirehpour, A. Arabi Shamsabadi, S. Khoshhal Salestan, M. Jabbari, M. Soroush, Simultaneous improvement of antimicrobial, antifouling, and transport properties of forward osmosis membranes with immobilized highly-compatible polyrhodanine nanoparticles, *Environ. Sci. Technol.*, 52 (2018) 5246–5258.
- [147] P. Lu, W. Li, S. Yang, Y. Wei, Z. Zhang, Y. Li, Layered double hydroxides (LDHs) as novel macropore-templates: The importance of porous structures for forward osmosis desalination, *J. Membr. Sci.*, 585 (2019) 175–183.
- [148] S. Xu, F. Li, B. Su, M.Z. Hu, X. Gao, C. Gao, Novel graphene quantum dots (GQDs)-incorporated thin film composite (TFC) membranes for forward osmosis (FO) desalination, *Desalination*, (2019) 219–230.
- [149] S. Lim, V.H. Tran, N. Akther, S. Phuntsho, H.K. Shon, Defect-free outer-selective hollow fiber thin-film composite membranes for forward osmosis applications, *J. Membr. Sci.*, 586 (2019) 281–291.
- [150] L. Deng, Q. Wang, X. An, Z. Li, Y. Hu, Towards enhanced antifouling and flux performances of thin-film composite forward osmosis membrane via constructing a sandwich-like carbon nanotubes-coated support, *Desalination*, 479 (2020) 114311. <https://doi.org/10.1016/j.desal.2020.114311>.